DISSERTATIONES CHIMICAE UNIVERSITATIS TARTUENSIS
117

DISSERTATIONES CHIMICAE UNIVERSITATIS TARTUENSIS
117

VLADISLAV IVANIŠTŠEV

Double layer structure and adsorption kinetics of ions at metal electrodes in room temperature ionic liquids

TARTU UNIVERSITY PRESS

Institute of Chemistry, Faculty of Science and Technology, University of Tartu, Estonia

Dissertation was accepted for the commencement of the degree of *Doctor philosophiae* in Chemistry at the University of Tartu on June 14th, 2012 by the Council of Institute of Chemistry, Faculty of Science and Technology, University of Tartu.

Supervisors: Prof. Enn Lust, University of Tartu, Estonia

Ph.D. Karmen Lust, University of Tartu, Estonia

Scientific consultant: Prof. Renat Nazmutdinov, Kazan State University, Russia

Opponent: Ph.D. Irina Petrushina, Technical University of Denmark
Commencement: August, 27th, 2012, Ravila 14A (Chemicum), rm 1021, 11:00

This work has been partially supported by graduate school "Functional materials and technologies" receiving funding from the European Social Fund under project 1.2.0401.09-0079 in Estonia.

ISSN 1406–0299
ISBN 978–9949–32–044–8 (trükis)
ISBN 978–9949–32–045–5 (pdf)

Tartu Ülikooli Kirjastus
www.tyk.ee
Tellimus nr 342

to my mentors:

T.I. Barna, V. Laur, V.V. Ossipov, R. Pullerits

Table of Contents

1. List of original publications....8
2. List of acronyms and notations....9
3. Introduction....10
4. Theoretical study of the electrical double layer at metal | aqueous solution interface....11
4.1. Methods and Models....12
4.1.1. Computational details....12
4.1.2. Dipole lattice model....13
4.1.3. H_2O and metal cluster models....14
4.2. Metal–H_2O bonding....16
4.2.1. Literature overview....16
4.2.2. H_2O adsorption energy, adsorption site and orientation....16
4.2.3. Metal–H_2O binding....17
4.3. Electrical double layer....19
4.3.1. Potential drop in the EDL....19
4.3.2. Theoretical model....21
4.3.3. Modelling results and discussions....22
4.4. Conclusive remarks....25
5. Adsorption of ions at Cd(0001) electrode from ionic liquid and aqueous solutions....26
5.1. Literature overview....26
5.1.1. Properties of RTILs....26
5.1.2. Electrical double-layer in RTILs....27
5.1.3. Temperature effect studies by EIS....28
5.2. Experimental....30
5.2.1. Experimental procedures....30
5.2.2. Differential, electrical double-layer and absorption capacitances. 31
5.3. Experimental results....32
5.3.1. Cyclic voltammetry....32
5.3.2. Nyquist (Z'', Z') and Bode (δ, f) plots....32
5.3.3. Capacitance....33
6. Discussions....38
6.1.1. Models of the EDL structure at electrode | RTIL interface....39
6.1.2. Theories of EDL at electrode | RTIL interface....40
7. Conclusions....43
8. References....44
9. Summary in Estonian....52
10. Acknowledgements....53
11. Publications....55

I. List of original publications

I. V. Ivaništšev, R.R. Nazmutdinov, E. Lust, A comparative DFT study of the adsorption of H_2O molecules at Bi, Hg, and Ga surfaces. Submitted to the Journal "Surface Science".

II. L. Siinor, C. Siimenson, V. Ivaništšev, K. Lust, E. Lust, Influence of cation chemical composition and structure on the double layer capacitance for Bi(111) | room temperature ionic liquid interface. Journal of Electroanalytical Chemistry 668 (2012) 30-36.

III. V. Ivaništšev, R.R. Nazmutdinov, E. Lust, Density functional theory study of the water adsorption at Bi(111) electrode surface. Surface Science 604 (2010) 1919-1927.

IV. L. Siinor, V. Ivaništšev, K. Lust, E. Lust, Impedance study of adsorption of iodide ions at Cd(0001) and Bi(111) electrode from various solutions with constant ionic strength. Journal of Solid State Electrochemistry, 14 (2010) 555-563.

Author's contribution:

Paper I: Performed all DFT calculations, analyses and modelling. Responsible for planning and writing of the manuscript.

Paper II: Performed all DFT calculations and analyses. Participated in writing of the manuscript.

Paper III: Performed all DFT calculations, analyses and modelling. Responsible for planning and writing of the manuscript.

Paper IV: Performed all electrochemical measurements at Cd(0001) electrode, modelling of the data and participated in interpretation of the results.

2. List of acronyms and notations

ab initio – a Latin term meaning "from first principles"
ac – alternating current
CV – cyclic voltammetry
DFT – density functional theory
EDL – electrical double-layer
EIS – electrochemical impedance spectroscopy
et al. – a Latin term meaning "and others"
in situ – a Latin term meaning in the context this work "localised at the interface"
MC – Monte-Carlo (simulation)
MD – molecular dynamic (simulation)
MSA – mean spherical approximation
PZC – potential of zero-charge
RTIL – room-temperature ionic liquid

δ – phase shift
R_{el} – electrolyte resistance
C_{dl} – electrical double-layer capacitance
C_{ad} – adsorption capacitance
R_{ct} – charge transfer resistance
Z_W – Warburg diffusion impedance

$EMIm^+$ – 1-ethyl-3-methylimidazolium cation
$BMIm^+$ – 1-butyl-3-methylimidazolium cation
$HMIm^+$ – 1-hexyl-3-methylimidazolium cation
$Py_{1,4}^+$ – 1-butyl-4-methylpyrrolidinium cation
BF_4^- – tetrafluoroborate anion
FAP^- – tris(pentafluoroethyl)trifluorophosphate anion
PF_6^- – hexafluorophosphate anion
Tf_2N^- – bis(trifluoromethylsulfonyl)imide anion

3. Introduction

Recently investigations of Room Temperature Ionic Liquids (RTILs) have become one of the popular trends in modern chemical research [1]. Due to their high stability under applied potential and their decisive role in electrochemical processes the RTILs at electrode interface attract considerable attention [2–4]. A detailed understanding of the structure, thermodynamics and kinetics of RTILs at the electrode surfaces is crucial for designing modern electrochemical devices, such as supercapacitors [5,6], actuators [7], batteries [8,9], solar cells [10], etc. Studies of RTIL based supercapacitors [11,12] and actuators [13,14] are performed at the University of Tartu. In our experimental research we aimed to provide new fundamental insights to the existing knowledge of the temperature dependences as well as to make new observations on adsorption kinetics at the Cd(0001) | $EMImBF_4$ and Bi(111) | $EMImBF_4$ interfaces [15,16]. We also initiated a series of systematic quantum chemical studies at the Density Functional Theory (DFT) level [17–19], which eventually led us to a better understanding of our previous experimental studies on iodide ion adsorption at Cd(0001) and Bi(111) electrodes from various aqueous solutions [20]. In this thesis we provide a comparative overview of the results for different systems, by presenting the most important conclusions as one logical conception of a structure–property correlation.

4. Theoretical study of the electrical double layer at metal | aqueous solution interface

So-called electrical double layer (EDL) at an electrical interface between an electrode and an electrolyte is the "heart" of electrochemistry. The paradigm of the EDL, established in the 20th century, has recently been dramatically changed in the light of new knowledge about the electrode | RTIL interface structure [21]. So far the EDL in various electrolyte solutions (besides RTILs) has been most extensively investigated at liquid mercury and gallium electrodes and solid bismuth, platinum and gold single crystal electrodes [22–25]. Even so, for metal | aqueous solution interface there are a number of unanswered questions and unexplained phenomena [26–28]. One of the unclear dependencies is the EDL compact layer capacitance dependence on the electronic and crystallographic properties of different metals.

For the last twenty years the adsorption processes and structure of the EDL at single crystal Bi(*hkl*) | electrolyte solution interfaces have been experimentally studied in order to examine contemporary, non-primitive, but still phenomenological theories and models of the EDL [29–35]. Lust *et al.* have noted that these theories are oversimplified and have pointed out the necessity of further developing of the theoretical models [33,35]. Recently Emets and Damaskin have summarised their long-term scrupulous experimental studies of the EDL at bismuth–gallium amalgam electrode in aqueous solutions and enlightened some problems concerning interfacial structure and quantitative properties [25,36,37]. In due course we started theoretical investigation of the molecular structure and dynamics at the bismuth | aqueous solution interface in order to estimate its microscopic properties. For this purpose, a water molecule and a Bi(111) surface, as research objects, and density functional theory (DFT) methods were chosen with a sensible goal to develop a better understanding about the interaction of the H_2O molecule(s) with the bismuth electrode surface and proceed further to more complicated systems [15,18,19].

As the most abundant solvent in nature and technology, water is involved in various physical and chemical processes related to corrosion, catalysis, electrochemical deposition, etc.; moreover it also plays a major role in various industrial processes, for example, in hydrogen production [38]. In our research we have studied and analysed such common properties of metal–H_2O system as adsorption sites, H_2O internal geometry, H_2O relative orientation and H_2O molecule adsorption energy. Afterwards, we focused on analysis of the nature of the bismuth– H_2O bond; investigated effects of solvation and electric field; applied a dipole lattice model in order to describe the first interfacial layer of water at the metal surface; and described H_2O clusters in contact with the Bi(111) face. The methods have been further extended for Ga(111), Bi(100), Bi(110), Hg(111) surfaces [18,19] in order to provide a wider comparison.

4.1 Methods and Models

4.1.1 Computational details

The quantum chemical calculations were performed using a B3LYP/LANL2DZ method, which implies Becke's three-parameter functional [39], Lee–Yang–Parr correlation functional [40] and Hay–Wadt effective core potentials [41]. The hybrid B3LYP functional was applied as implemented in the Gaussian 03 and 09 program codes [42,43]. Additional polarisation functions were used for the double-ξ basis sets of metal (LANL2DZ), hydrogen and oxygen (6-31G) atoms [44,45].

The metal–H_2O adsorption energy (ΔE_{ad}) was calculated as:

$$\Delta E_{ad} = E_{\text{cluster-}H_2O} - E_{\text{cluster}} - E_{H_2O} \quad (1)$$

where E denotes the total energy of a system, which depends on interfacial geometry and orientation of the adsorbate, and on applied electric field (F). The internal geometry of the H_2O molecule was defined by O–H distance (r) and H–O–H angle (α). The orientation of H_2O was described by z_0 and θ, where z_0 is the optimised distance calculated from the position of the first cluster layer to the O-atom, and tilt angle (θ) describes the H_2O molecule orientation relative to the surface normal (Fig. 1). The electric field was treated via finite-field DFT method implemented in the Gaussian program suite [42,43]. The sign of the field in a direction perpendicular to the surface was chosen so that a positive sign induces a small negative charge on the H_2O molecule and the model cluster corresponds to a positively charged surface. We examined the effect of the electric field on three different orientations of the H_2O molecule: parallel to the surface (H-par, θ = 90°); H-atoms pointed towards the surface (H-down, θ = 180°), and O-atom pointed towards the surface (H-up, θ = 0°, shown in Fig. 2b). The obtained data were used for statistical-mechanical modelling of a H_2O monolayer according to the dipole lattice model.

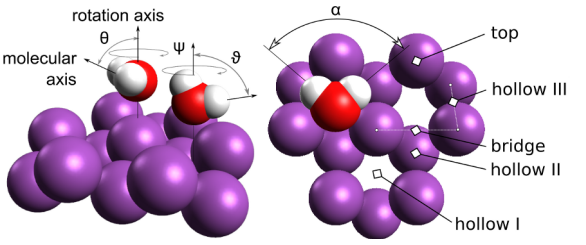

Figure 1. Side and top views on the different adsorption sites at the model cluster used to describe the H_2O molecule adsorption at the Bi(111) surface. The bond angle (α) characterises the internal geometry of the molecule. The rotation angles (θ, ϑ and ψ) characterise the orientation of the molecule relative to the surface normal labelled as "rotation axis".

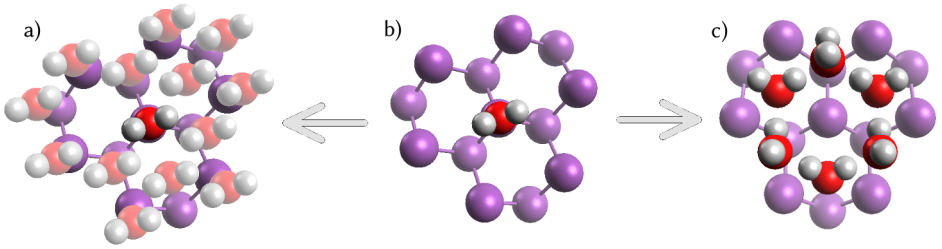

Figure 2. a) In the dipole lattice model each H_2O molecule is represented as a dipole, while the metal–H_2O interaction of the central molecule is described at DFT level. The empty site near the central molecule represent a defect in the dipole lattice, which is described by parameter ξ. The ξ value of 0.6 corresponds to the ice-like structure, in which only two third of favourable sites are occupied.
b) top view on a single H_2O molecule adsorbed at the bismuth cluster in the H-up orientation. c) a part of the ice-like structure at the Bi(111) surface.

4.1.2 Dipole lattice model

The dipole lattice model, developed by Schmickler [46] and Fawcett [47], describes the behaviour of solvent molecules at a polarisable interface [48–50]. For a long time an uninvestigated aspect of the model has been the chemical interaction between a given metal surface and the modelled H_2O monolayer. Only recently the progress in DFT methods has made it possible to account for metal–H_2O interaction in the dipole lattice model [19,51]. By using this model we assumed that a single H_2O molecule in an effective mean-field describes the metal–H_2O interface properties. The effective field (F) was expressed as:

$$F = \frac{I\xi\langle s\rangle}{\mu}, \tag{2}$$

where $I\xi$ is the energy of electrostatic interaction of a given H_2O dipole with the dipoles of all other modelled molecules, $\langle s\rangle$ is a dimensionless parameter depending on the effective field F and showing whether H-up or H-down orientation is predominant, and μ is the dipole moment of the H_2O molecule.

The electrostatic interaction energy depends on the dipole lattice topology and the distance between the dipoles (l):

$$I = \frac{1}{4\pi\varepsilon_0}\sum_i \left(\mu^2/l_i^3\right). \tag{3}$$

The $\langle s\rangle$ values were calculated numerically in accordance with:

$$\langle s\rangle = \frac{x^2 H^{\text{H-up}} - H^{\text{H-down}}}{x^2 H^{\text{H-up}} - xH^{\text{H-par}} - H^{\text{H-down}}}, \tag{4}$$

where $H^i = \exp(-\Delta E_{\text{ad}}^i / k_{\text{B}}T)$, $x = \exp(-\mu F / k_{\text{B}}T)$, k_{B} is the Boltzmann constant and T is the absolute temperature. Evaluated parameters were used for further analysis presented in section 4.3.3. More details are given in Refs. [19,52].

4.1.3 H_2O and metal cluster models

In order to test the influence of lateral interactions on the adsorption properties of H_2O, we performed DFT calculations with a cluster consisting of 13 H_2O molecules (Fig. 2). In this model the H_2O molecules form the so-called ice-like structure, which is more rigid than the structure treated by the dipole lattice model. The main advantage is that the local hydrogen-bonding is accounted directly at the DFT level, however, the long-range dipole–dipole interactions are neglected.

The binding energy of the central molecule with the metal surface was calculated according to Eq. 1, and an average H-bond energy was estimated as:

$$\Delta E_{\text{H-bond}} = \left(E_{13\text{H}_2\text{O}} - E_{7\text{H}_2\text{O}} - E_{6\text{H}_2\text{O}} \right) / 15, \tag{5}$$

where "13 H_2O", "7H_2O" and "6H_2O" stand for three parts of the 13 H_2O cluster containing thirteen, seven and six H_2O molecules, respectively.

We investigated the dependence of the binding and hydrogen-bonding energies on the O–O distance, relaxing the internal geometry and relative orientation of the H_2O molecules in cluster. The eight optimised parameters were: O–H distance (r), H–O–H angle (α), metal–OH_2 tilt angle (θ and ϑ in Fig. 1), and metal surface–O distance (z) for two different types of adsorbed H_2O molecule orientations (Figs. 2c and 3).

The calculated values of the binding energy and the H_2O–H_2O interaction energy have an accuracy of ±4÷±6 kJ mol^{-1} at B3LYP/DFT level [53]. The range of ±4 kJ mol^{-1} is comparable to the difference in the internal energy of liquid water and ice [54], and such inaccuracies in theoretical calculations have only been overcome recently with the help of different DFT functionals by introducing correction to van der Waals interactions [55,56]. Our tests for the long-range interactions correction showed that at CAM-B3LYP/DFT level [57,58] it somewhat compensates for the computational correction of basis set superposition error. Thus, we didn't aim to make more accurate estimations in the present research bearing in mind that for more precise quantitative agreement with experiment [35] the zero-point energy and the entropy difference corrections should also be taken into account. On the other hand, the accuracy of the presented data is sufficient for comparative modelling of the interfacial H_2O layers using the dipole lattice model.

The metal surfaces were modelled by clusters. In a chosen face-centred cubic packing the nearest Ga atom–atom distance (0.29 nm) refers to a peak position on the radial distribution function plot for gallium [59]. Similar distance parameter for Hg equals 0.30 nm [60]. These distances are comparable to the ones characterising common *d*- and *sd*-metals (Fig. 4) [61]. The bismuth (*hkl*) surface (in rhombohedral notation) was modelled by clusters for which the distance and the angle between neighbouring metal atoms (within the surface layer) is equal to the Bi bulk values (0.307 nm, 95.54°, Fig. 5) [62].

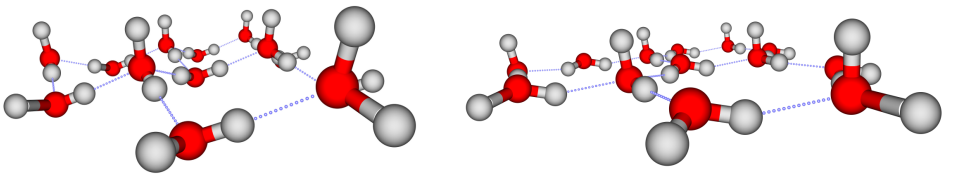

Figure 3. Optimised geometry of the 13 H_2O cluster at the modelled Bi (left) and Ga (right) surfaces. Fifteen OH···O hydrogen bonds are marked with dotted lines. The metal clusters are not shown for clarity.

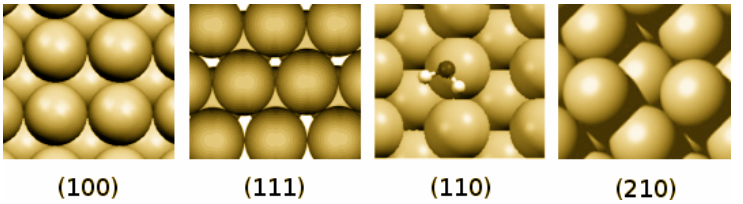

Figure 4. Top view of the Me(100), Me(111), Me(110) and Me(210) faces. A water molecule is shown for comparison. Among most studied *sd*- and *d*-metals the metallic radii vary from the smallest value of 0.125 nm for Ni to the largest value of 0.15 nm for Au. Metallic radii for Hg and Ga are 0.15 and 0.145 nm, respectively.

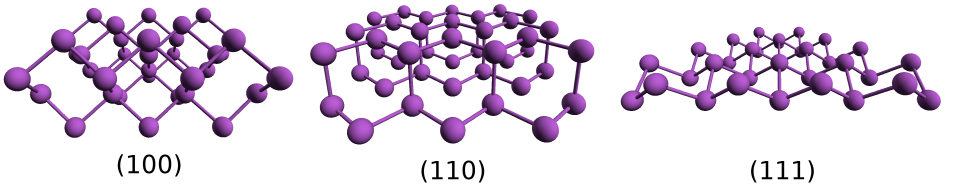

Figure 5. At the modelled (100), (110) and (111) faces of a bismuth single crystal in case of the H_2O molecule adsorption the "hollow" site was found to be energetically as preferable or even more than the top site. For the hollow site the calculated at B3LYP/LANL2MB leve adsorption energy values equal to −29, −24, −20 kJ mol^{-1} for the Bi(111), Bi(110) and Bi(100) faces, respectively. For the top site the adsorption energy values are equal to −14, −25, −18 kJ mol^{-1} for the same sequence of planes modelled by Bi_{33}, Bi_{42}, and Bi_{34-38} clusters, respectively.

Figure 6. ΔE_{ad},θ-dependence for the top (●) and hollow (▾) sites at the Bi(111) surface. A reorientation barrier less than $2k_BT$ is seen for the top site. Much higher reorientation energy is characteristic for the hollow site as well as, in general, for the favourable sites at Bi(111), Ga and Hg surfaces studied [18].

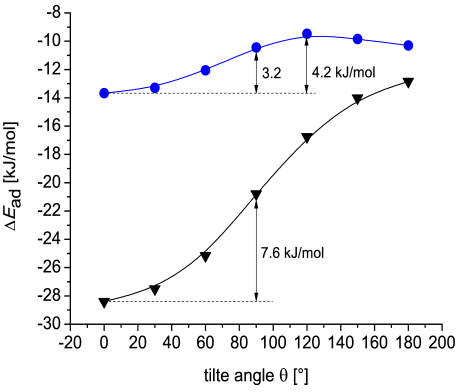

4.2 Metal–H_2O bonding

4.2.1 Literature overview

The majority of computational investigations have been devoted to the description of H_2O behaviour at Pt(*hkl*) [63–74], Pd(*hkl*) [75–80] and Cu(*hkl*) [81–91] faces. Smooth (100, 111) [64,68,75,81,86,92–99] and stepwise (111, 210, etc.) [65,67,82,85,100,101] compact faces have mainly been studied. This much attention has been devoted to *d*- and *sd*-metals due to a persistent need for cheaper catalysts and higher efficiencies in industrial chemical syntheses. Less attention has been devoted to catalytically inactive *sd*- and *p*-metals [99,102–104]. We have investigated H_2O adsorption characteristics at Bi(111) [19], Ga and Hg [18] surfaces. The comparison with the previous studies for Ga and Hg surfaces [51,52,105,106] is given in Ref. [18]. The results of all other studies are summarised in several reviews (for example, Refs. [38,107,108]) and in a large number of comparative studies [66,99,109–115]. Main features characterising the adsorption of H_2O at metal surfaces are summarised as:

1. At positive and close to zero surface charge values a single H_2O molecule adsorbs through the oxygen atom to the surface, while at negative – through the hydrogen atom(s). The preferable position and orientation depends on the distribution of the electron charge density near the metal surface. In terms of soft–hard acids and bases conception a soft H_2O molecule can be readily polarised and accordingly occupies "soft" surface regions. The bond angle and bond lengths for the adsorbed H_2O molecule are only slightly perturbed from the corresponding values obtained in "vacuum";

2. The adsorption energy of H_2O varies in a narrow interval from −10 to −50 kJ/mol, comparable to the hydrogen-bonding energy (−28 kJ/mol) calculated at the same level of theory. In terms of frontier molecular orbital approach, the bonding is formed by the interaction of the metal orbitals with the $1b_1$ molecular orbital of H_2O [47,52,56,57]. In more general terms of electron charge density, the donation and back-donation resulting in a redistribution of the electron charge density is characteristic for the H_2O adsorption at metal electrodes.

4.2.2 H_2O adsorption energy, adsorption site and orientation

On the (111) plane of a bismuth single crystal the "hollow" site was calculated to be energetically preferable for the H_2O adsorption (−31 kJ mol^{-1}, z_0 = 0.23 nm). For the Ga and Hg surfaces the top site was confirmed to be energetically the most favourable adsorption site: ΔE_{ad}(H-up) and z_0 values are equal to −25 kJ mol^{-1}; 0.27 nm and −36 kJ mol^{-1}; 0.30 nm, respectively. Thus, due to specific atomic corrugation, the distance between favourable sites

increase in a sequence: Bi surface (0.26 nm) < Ga surface (0.29 nm) < Hg surface (0.30 nm). However, in contrast with the H_2O adsorption on mercury and bismuth, at the Ga surface the bridge, hollow and ontop sites are almost equally energetically favourable according to the calculated adsorption energy values. This can be seen from averaged adsorption energies, given in Table 1.

The reorientation energies (Fig. 6) describe the ability of the H_2O molecule to change its orientations under applied electric field. The energy of H_2O reorientation at Hg is noticeably higher (17 kJ mol^{-1}) compared to those calculated for the favourable positions at the surfaces of Ga (10 kJ mol^{-1}) and Bi(111) (14 kJ mol^{-1}). The dependence of the metal–H_2O interaction energy on the tilt angle (θ) at the surfaces of Bi(111) and Hg indicates that the H_2O molecule is bound preferentially through the O-atom in an orientation perpendicular to the surface plane (H-up) [18]. Herewith, the energy difference for tilting by 60° is comparable with the thermal fluctuation energy at room temperature (k_BT = 2.4 kJ mol^{-1}) [18]. For the Ga surface a tilted orientation (60°) is most preferable. Herewith, over a range of ±60°, the energy difference for tilting is comparable to k_BT. The calculated adsorption energy dependences on the surface charge density were used in further analysis using the dipole lattice model. Looking ahead (in section 4.3.3) we conclude, that lower reorientation energy significantly influences the capacitive properties of the interface between metal surface and electrolyte solution.

Table 1. Averaged adsorption energies (kJ mol^{-1}) of H_2O in H-up orientation at optimised z_0 distances, and estimated reorientation energies ($\Delta\Delta E_{ad}$, in kJ mol^{-1}) for different adsorption sites. $\Delta\Delta E_{ad}$(H-up/down) = ΔE_{ad}(H-down) – ΔE_{ad}(H-up). Data for Bi electrode was calculated using the B3LYP/LANL2DZ method [19], while for Ga and Hg the B3LYP/LANL2DZ was employed [18]. The difference in results for two methods is small in case of bismuth [18].

clusters	site	z_0, nm	$-\Delta E_{ad}$(H-up)	$\Delta\Delta E_{ad}$(H-up/down)
Bi_{10-24}	top	0.35	16	
Bi_{24-46}	hollow	0.23	27	14
Bi_{10-24}	hollow II	0.22	22	
Ga_{7-71}	top	0.26	23	10
Ga_{31-34}	bridge	0.28	22	
Ga_{31-34}	hollow	0.30	22	
Hg_{7-71}	top	0.30	34	17
Hg_{31-34}	bridge	0.30	27	
Hg_{31-34}	hollow	0.31	27	

4.2.3 *Metal–H_2O binding*

According to one of the generally accepted explanations, the metal–H_2O bonding originates due to a charge donation from the oxygen lone pair to the unoccupied orbitals of the metal and back donation from the filled orbitals of the metal to the unoccupied orbital of H_2O [116]. For the top site of most metals the overlap of the lone-pair orbital with metal *p*- and *d*-orbitals is

the largest. Thus, the localised metal–H_2O bond is stronger. For H_2O molecules the adsorption properties of the energetically preferable hollow site at the Bi(111) surface significantly differ from those at other close-packed metal surfaces. At close-packed *d*-metals, a single H_2O molecule lies almost parallel to the surface, but at the Au(210) [101], Hg [18,52] and Bi(111) [18,19] surfaces it tends to adsorb perpendicular to the surface.

In the framework of the DFT it is mostly justified to address these findings to the electron charge density distribution of a systems. Two-dimensional maps of the electron charge density display a clear difference between the adsorption sites at the Bi(111) and Hg surfaces (Fig. 7). We calculated the volume integral of electron charge density over a sphere with a diameter of 0.3 nm and at z_0 height above a given surface site in order to amplify the difference. The electronic population inside of such a sphere may be considered as a criterion for the donor–acceptor properties of the surface site. As can be seen from Table 2, higher electronic population corresponds to the preferable adsorption sites – hollow for the Bi(111) surface and top for Ga, Hg and In. As a consequence of the electron charge density inhomogeneity these sites appear to be softer centres, at which the electron charge density can be easily removed or added most easily [66].

Table 2. Volume integrals (in relative units) of electronic density over sphere with a diameter of 0.3 nm at optimised distance z_0 coaxial with a given surface site.

	top	bridge	hollow	hollow II
Bi	0.3	0.79	1	0.39
Ga	1	0.09	0.16	
Hg	1	0.67	0.93	
In	1	0.18	0.23	

One of the fundamental chemical principles states that either hard–hard or soft–soft interactions are preferred when two reactants interact with each other. Thus, a soft H_2O molecule prefers distinct regions of "softness" for binding to the surface. The electron charge density redistribution is elucidated (Fig. 8) by the charge density difference $\Delta\rho$:

$$\Delta\rho = \rho_{\text{cluster-}H_2O} - \rho_{H_2O} - \rho_{\text{cluster}}, \quad (6)$$

where ρ denotes the total charge density of a system.

The depletion of charge density in the region between a given metal surface and the H_2O molecule adsorbed ontop becomes stronger in the row of metals: Bi < Ga < Hg < Pt. In agreement, larger changes are observable for H_2O adsorption at the preferable hollow site on the Bi(111) surface, than at the top site. The absolute value of the adsorption energy increases in the same order. The general picture of the metal–H_2O bonding in terms of charge redistribution (i.e. polarisation) is simple: the contact region is depleted while the inner regions of the H_2O molecule and metal cluster gain the electron charge density, resulting in a lower system energy. The depletion is explained

by Pauli repulsion, which simply means that two overlapping filled orbitals cannot form new stable orbitals (Pauli exclusion principle). Furthermore, if an orbital concept is used, the depletion and gain can be divided into a charge donation from the oxygen lone pair to the unoccupied orbitals of the metal (that is depletion in the lone pair location) and back donation from the filled orbitals of the metal (the depletion above the adsorption site) to the unoccupied orbital of H_2O (gain in the H_2O molecule inner region, shown in blue colour in Fig. 8).

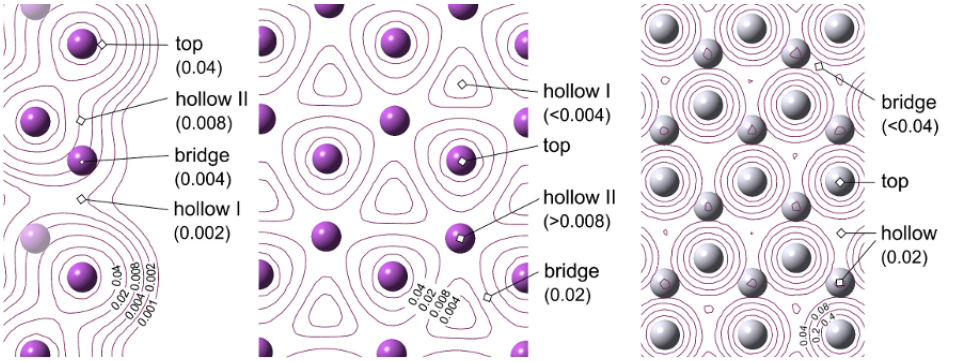

Figure 7. Contour maps of the electron charge density in the direction of Bi(111) surface normal (left), perpendicular to the Bi(111) surface normal (centre), and perpendicular to the Hg surface normal (right). The planes were chosen to cross the metal nuclei of Bi (left and centre) and Hg (right) surfaces as shown. The density (in atomic units) increases in value from the outermost 0.001 contour inwards in steps of $2{\cdot}10^n$, $4{\cdot}10^n$, and $8{\cdot}10^n$ with n starting at −3.

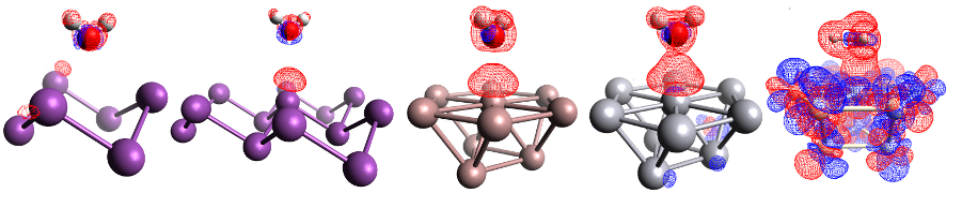

Figure 8. 0.002 a.u. isosurfaces of the electron charge density difference for H_2O at the Bi(111) hollow, Bi(111) top, Ga top, Hg top and Pt top surface sites, respectively from left to right. Charge depletion is shown in red and charge gain – in blue. A very strong $\Delta\rho$ at the Pt cluster is probably caused by so-called cluster size effect. Only part of the Bi_{24}, Ga_{31} and Hg_{31} and Pt_{16} clusters is shown for clarity.

4.3 Electrical double layer

4.3.1 Potential drop in the EDL

Electrified interfaces represent the principal object of electrochemistry. Various aspects of this area are described in details in reviews and textbooks [22,26,117]. Let's start from a basic relationship of a possible potential drops

at the metal/solution interface [23,118]: $\Delta^{s}_{Me}\psi = \Delta\phi - \chi^{s}_{Me} + \chi^{i}_{s}$, where $\Delta\phi$ is the surface potential at the metal–solution interface, χ^{s}_{Me} is the potential drop in the metal surface layer in contact with the solvent molecules, and χ^{i}_{s} is the potential drop in the solvent surface layer. The presence of the solvent molecules changes the distribution of the electrons at the surface, and the interaction of the solvent molecules with the metal surface can lead to a small net reorientation of the molecules dipoles. Denoting these changes in the surface potentials by $\delta\chi^{s}_{Me}$ and $\delta\chi^{i}_{s}$, we have: $\Delta^{s}_{Me}\psi = \delta\chi^{s}_{Me} - \delta\chi^{i}_{s}$. It is convenient to consider the potential drop at the potential of zero charge (PZC, $E_{q=0}$), and to use mercury electrode as a reference electrode [23,25]:

$$\Delta^{Hg}_{Me}E_{q=0} \approx \Delta^{Hg}_{Me}\psi + \left(\Delta^{Hg}_{Me}\delta\chi^{s}_{Me} - \Delta^{Hg}_{Me}\delta\chi^{i}_{s}\right)_{q=0}. \quad (7)$$

Here and further below the potential drop in the diffuse layer [118] is neglected. $\Delta^{Hg}_{Me}\psi$ is equal to the difference of work functions of the metals. $\delta\chi^{s}_{Me}$ appears due to extending of the electron charge density outside from the ionic skeleton of the metal (the so-called "electronic tail") and its interaction with solvent molecules. The metal surface charge density distribution is analogous to common electrified interfaces representing two oppositely charged spatial regions with zero overall charge. The absolute potential drop $\delta\chi^{s}_{Me}$ across this regions (influenced by the interfacial layer of water) was estimated accordingly:

$$(\delta\chi^{s}_{m})_{q=0} = (\varepsilon^{Me}_{HOMO} - \varepsilon^{Me\text{-}s}_{HOMO})/F, \quad (8)$$

where ε^{Me}_{HOMO} and $\varepsilon^{Me\text{-}s}_{HOMO}$ are energies of the highest occupied molecular orbital (HOMO) for the metal cluster and the adsorption complex, respectively; and F is the Faraday constant.

A significant $\delta\chi^{i}_{s}$ potential drop is created by the formation of a dipole layer along with the generation of a charged surface–counter-ion bilayer. This potential drop can be divided into components $\delta\chi_{s}$ and $\delta\chi_{i}$, representing the interfacial dipole layer and the ionic capacitor, respectively. The latter accounts for the interaction of ions with their image charges in the metal surface layer. Describing the $\delta\chi_{i}$ changes, we assumed that the image plane position is effectively defined by the metallic electron charge density located at a half of the metal interlayer distance from the surface plane [48,119]. Potential drop in the surface layer of water molecules was estimated in accordance with:

$$\delta\chi_{s} = \rho_{s}\langle\mu_{\perp}\rangle = -\frac{\rho_{s}\langle s\rangle\mu}{\varepsilon_{0}}, \quad (9)$$

where ρ_{s} is the surface density of the H_2O molecules and $\langle\mu_{\perp}\rangle$ is the averaged dipole moment normal projection in the H_2O monolayer.

4.3.2 Theoretical model

The analysis for calculation of relative potentials drops was presented in a recent paper [18]. Below we discuss the dependence of capacitance on the surface charge density obtained in combination of DFT calculations and the dipole lattice model.

Under certain assumption, the differential capacitance of the EDL compact layer (so called Helmholtz capacitance, C_H) is expressed as follows:

$$\frac{1}{C_H}=\frac{\partial\delta\chi_H}{\partial\sigma}=\frac{\partial\delta\chi_i}{\partial\sigma}-\frac{\partial\delta\chi_s}{\partial\sigma}-\frac{\partial\delta\chi^s_{Me}}{\partial\sigma}=\frac{1}{C_i}-\frac{1}{C_s}-\frac{1}{C_{Me}}. \tag{10}$$

As was mentioned above and shown in Fig. 9 there are three regions of charge density segregation, i.e. the surface region can be effectively divided into three capacitors. The metal capacitance (C^s_{Me}) is defined as:

$$C^s_{Me}=\frac{-\partial\sigma}{\partial\delta\chi^s_{Me}}\approx -F\frac{\partial\sigma}{\partial\varepsilon^{Me}_{HOMO}}. \tag{11}$$

The solvent layer capacitance (C_s) is expressed as:

$$C_s=\frac{-\partial\sigma}{\partial\delta\chi_s}=\frac{\varepsilon_0}{\rho_s\mu}\frac{\partial\sigma}{\partial\langle s\rangle}. \tag{12}$$

The capacitances are given in μC cm^{-2} and defined to have positive values according to Eq. 10.

The ionic capacitor (C_i) refers to the capacity was treated as an idealised parallel-plate capacitor:

$$C_i=\frac{\partial\sigma}{\partial\delta\chi_i}=\frac{\varepsilon_0}{d}, \tag{13}$$

where ε_0 is the permittivity of vacuum, d is the distance from the image plane to the counter-ions. This distance was approximated as a sum of a weighted average z_{avg} value for H_2O near a given surface in H-down, H-par and H-up orientations and a distance of closest approach of the counter-ion. The population of the H_2O orientations was taken into account to estimate z_{avg}. Calculations using the 13 H_2O cluster model and a single hydrated ion indicate that the distance of closest approach of the ion is approximately 0.5 nm from the surface plane (Fig. 10). Herewith, the second layer of the H_2O molecules in the 13 H_2O bilayer at the Bi(111) face is situated at 0.35 nm above the surface, while the first layer – at a smaller distance of 0.25 nm (Figs. 3 and 10). All molecules in the 13 H_2O cluster are situated at the same distance (0.35 nm) above the Ga and Hg surfaces (Fig. 3). Thus we might anticipate that from geometrical point of view the counter-ion has a possibility to somehow move closer towards the Bi(111) surface, while it is compelled to locate at a slightly

larger distance from the Hg and Ga surfaces. The distance values obtained by Molecular Dynamic simulations [120–123] are systematically lower (from 0.3 to 0.4 nm) than the ones estimated for the 13 H_2O cluster model. The agreement between different approximations is seen in an observation that the counter-ion is situated above the first interfacial water layer.

To sum up, we used Me_n–H_2O cluster models to estimate the C^s_{Me} values at DFT level; combined the DFT results with the dipole lattice model in order to obtain the C_s values; and used empirical d values in order to calculate C_i. We applied the electric field (section 4.1.1) and derived C_H dependence on charge density from −4.55 to 4.55 μC/cm^2 for Ga, Bi(111) and Hg electrodes. The experimentally obtained compact layer differential capacitance values are shown in Fig. 11a. Going from negative to positive potentials the capacitance values increase more rapidly for gallium, than for Bi and Hg [23]. Much higher capacitance of the EDL at gallium in aqueous solutions [25,124] was previostly explained, for instance, by the chemisorption of H_2O at the Ga electrode [125], or by the higher electronic charge density at gallium metal [26].

4.3.3 Modelling results and discussions

It is interesting to point out that based on our very first computational results the increase of the modelled capacitance was reproduced [17]. However, it appeared to take place at positive surface charge densities, where water molecules react with the gallium electrode. During more systematic search among combinations of LANL2DZ, 6-31G**, 6-311G**, aug-cc-pVDZ functionals for H and O with LANL2DZ, LANL2MB, ECP60MWB, AUG-CC-PVDZ, 6-31G** and 6-311G** for metal atoms the more reliable DFT results were obtained.

Yet, the modelling based on more reliable DFT results seemed to somehow wrongly describe the capacitance behaviour modelled in the range from −4.55 to 4.55 μC/cm^2, until the computational results were extrapolated to the conditions of higher absolute values of the surface charge density. The obtained C_H,σ-dependences, shown in Fig. 11b, were plotted using the following values: 0.135 nm (Bi) or 0.15 nm (Ga, Hg) for counter-ion position in addition to the calculated z_{avg} value. The effective distance of closest approach of counter ions to the Bi(111) surface (0.42 nm) is lower than could be predicted for the 13 H_2O cluster model, suggesting that the counter-ion might come closer to the Bi(111) surface and coordinate with (i.e. become hydrated by) the interfacial layer of the H_2O molecules.

The capacitance peaks in C_H,σ-dependence lies far above experimentally measurable surface charge densities, except for mercury (Fig. 11). An important feature is striking: a hump at C_H,σ-dependence for Ga | solution interfaces is observed at negative σ values. The position of the hump depends only on the calculated adsorption energies, while the absolute values of the capacitance depend on empirical distance parameter used. We address the origin of the hump to the reorientation of the adsorbed H_2O molecules. In this conclusion the population dependence (Fig. 12) on the surface charge density for

the H-down, H-par and H-up H_2O orientations is considered. The H-par orientation population (in the framework of the dipole lattice model) is indirectly related to the averaged normal projection of the dipole moment in the dipole layer ($\langle \mu_\perp \rangle$, Eq. 9). The greater the change in the H-par orientation population, the higher is the change of $\langle \mu_\perp \rangle$. In accordance with Eqs. 10 and 12, if the solvent capacitance values are smaller, the total compact layer capacitance is higher.

It is interesting to discuss different explanations. The chemisorption of H_2O at the Ga surface was believed to result from a smaller distance of the solvent dipoles closest approach to the metal surface, in such way initiating the rise of the C_H capacitance [25]. In another explanation, the denser electronic tail has been shown to cause stronger repulsion of molecules attached to the Ga surface (under some restrictions of the model) [26] and to provoke the capacitance increase. It should be noted that both claimed effects were partially found to be true in our research. As it has been shown in section 4.2.3, the H_2O adsorption at the Ga and Pt(*hkl*) surfaces has more characteristic attributes of chemisorption, than at the surfaces of Bi(111) and Hg. We also showed in Ref. [18] that among the metals studied, only in the case of gallium, the metal capacitance (Eq. 11) is strongly influenced by adsorption of the H_2O molecules. Nevertheless, the presented results and analysis enlighten the dominant role of the interfacial solvent layer on the total interfacial properties of metal | electrolyte solution interface.

It must be admitted that our approach is not truly self-consistent, as we use semi-empirical distance parameter for the distance of closest approach of the counter-ion. Fawcett and Ryan have recently driven attention to the difference in the ionic radii and its impact on the potential drop [126]. The authors have shown that contact adsorption of perchlorate anion does not need to be invoked to explain the capacitance values observed at mercury. Interestingly, small changes in the distance parameter in our model may result in higher capacitance value, which are usually explained by contact adsorption. However, the changed distance parameter still corresponds to the position of the counter-ion outside the first interfacial layer of the H_2O molecules. This conspicuous feature is shown in section 6.

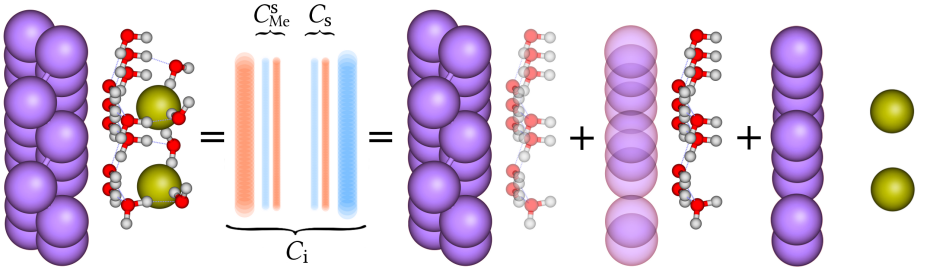

Figure 9. Division of the metal | electrolyte solution interface into charge density segregation regions, which are characterised by metal, solvent and ionic capacitances.

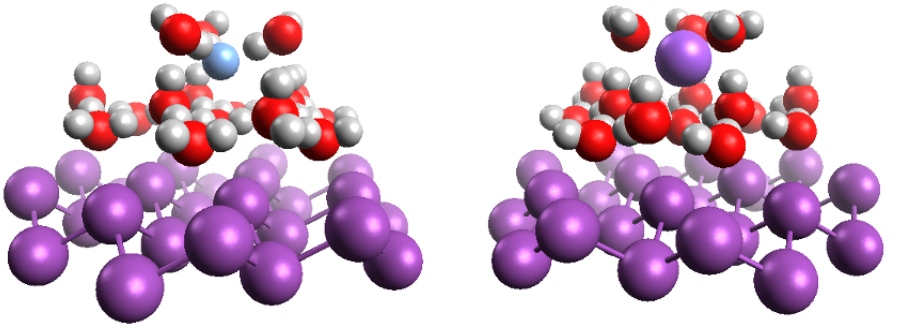

Figure 10. Bi_{24}–$(H_2O)_{13}$–$F^-(H_2O)_3$ model (left), Bi_{24}–$(H_2O)_{13}$–$Na^+(H_2O)_3$ model (right). The second layer of the H_2O molecules in the 13 H_2O bilayer at the Bi(111) face is situated at 0.35 nm, while the first layer – at 0.25 nm above the surface.

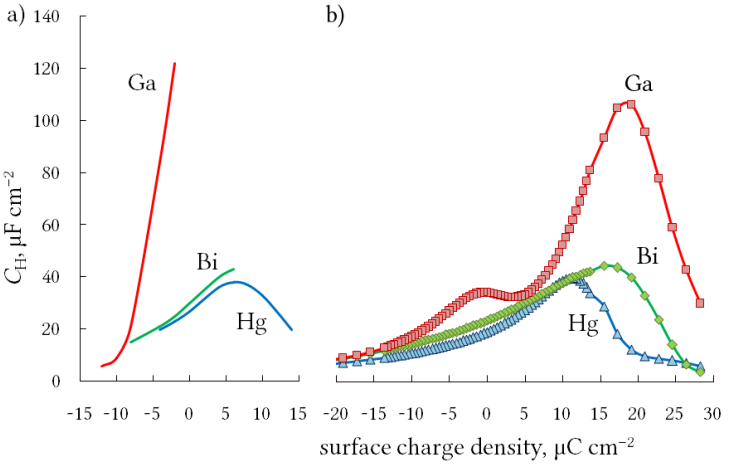

Figure 11. a) Experimental C_H,σ-dependence for Ga, Bi and Hg [25,26,35]. b) Theoretical C_H,σ-dependence for Ga, Bi and Hg.

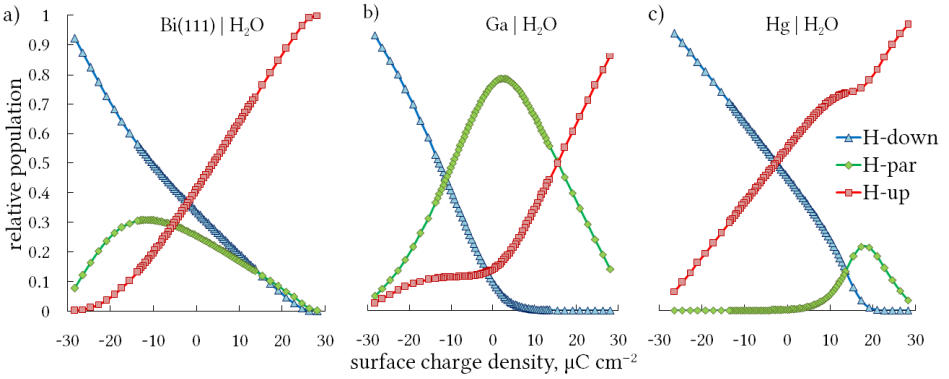

Figure 12. The dependence of H_2O population on the surface charge density for a given H_2O orientation at a) Bi(111), b) Ga, c) Hg surfaces.

4.4 Conclusive remarks

The objective of this theoretical research [18,19] was to develop a simple model that would: 1) account for interactions of the H_2O molecule with the metal surfaces, through H-bonds wit neighbouring molecules and with solvent dipoles at a long-range; 2) predict reliable potential drop values across the interface; and 3) describe the EDL compact layer capacitance at the metal | electrolyte interfaces modelled. The theoretical representation of the EDL structure, potential drop component values and corresponding artificially separated capacitors enabled us to model the differential capacitance behaviour at different metal | electrolyte solutions interfaces. According to the dipole lattice model the properties of H_2O in the first interfacial layer mainly determine the compact layer capacitance values. This observation is also confirmed by the 13 H_2O cluster model calculations published in Ref. [18]. The results established lead us to an important conclusion that it is not the accumulation of counterions forming parallel-plate capacitor, which solely governs the total differential capacitance of the compact layer, but the sum of different smaller capacitors appearing due to polarisation of the interface and influenced by lateral interactions. This conclusion is probably transferable onto more sophisticated systems, such as the EDL at electrode | room temperature ionic liquid interface, which is discussed in section 6.

5. Adsorption of ions at Cd(0001) electrode from ionic liquid and aqueous solutions

In electrochemistry, adsorption is an increase in the concentration of ions at an interface of an electrode and an electrolyte (solution) due to the operation of surface forces [127]. This phenomenon occurs in every single stage of a heterogeneous electrochemical reaction and its role in electrochemical reactions changes upon any variation of electrode potential and temperature. Examination of the temperature effects, in addition to the electrode potential influence, is thence of crucial importance for practical purposes, primarily for the development of batteries and fuel cells and also for the development of modern electrosynthesis methods, corrosion protection, etc. [128]. During the 20th century electrochemical reactions were mainly carried out in the aqueous solutions. Nowadays, a new class of non-aqueous RTILs serve as a perspective electrolyte for the electrochemistry of the future [2,3]. In the light of new prospects, however, we must admit that the kinetics of adsorption even in aqueous solutions is still not fully understood. Just a decade ago the kinetics of specific adsorption of ions at single-crystal electrodes was a hot trend in electrochemical research. Some studies were devoted to the phenomena of "capacitance dispersion" revealing a complexity of the adsorption. During this research experimental studies of iodide adsorption at Cd(0001) and Bi(111) from aqueous solutions have been performed [20]. Later, similar studies were performed in RTILs [15,129,130]. For the aqueous electrolytes it was shown that the adsorption step with partial charge transfer from the iodide ion to the electrode surface is the slowest rate determining step [20]. The remarkable similarity in kinetics of the ions adsorbing from aqueous solutions and RTILs at the Cd(0001) and Bi(111) electrodes has been demonstrated, which was also emphasised in the most recent works of Kolb *et al.* using Au(*hkl*) electrodes [131,132]. All the more interesting, our studies reveal a clear difference in the differential capacitance (C_d) dependence on temperature for metal | aqueous electrolyte solutions and metal | RTIL electrodes. For a simple comparison the Electrochemical Impedance Spectroscopy (EIS) method has been applied in order to characterise the C_d,T-dependence at the Cd(0001) | 1-ethyl-3-methylimidazolium tetrafluoroborate ($EMImBF_4$) and Cd(0001) | $0.1x$ M KI + ⅓×0.1(1 − x) M Na_2SO_4 interfaces.

5.1 Literature overview

5.1.1 Properties of RTILs

RTILs are defined as liquid below 100℃ salts composed entirely of organic cations and organic or inorganic anions [4]. A tendency to crystallise at low temperatures results from the flexibility of anions and asymmetry of cations [3]. The most common RTILs are based on pyridinium, imidazolium,

phosphonium, or ammonium cations, combined with anions such as BF_4^-, PF_6^-, NO_3^-, $CF_3SO_3^-$, etc. [4]. As RTILs are composed of interchangeable ions, they may undergo almost unlimited structural variability [3].

Physical properties of an RTIL strongly depend on the chemical structure of ions. For instance, viscosity is determined by electrostatic interactions, van der Waals forces and hydrogen bonding between the ions. Precisely as may be anticipated, RTILs with lower viscosity have higher conductivity.

Consideration of the structural aspects of RTILs, especially their structure near the electrode surface, is crucial for the rationalisation of electrochemical processes in RTILs. Such processes at the RTILs | electrode interface include: diffusion (mass transport), adsorption at the interface (change in surface excess), and charge transfer process across the interface. Experimentally they can be characterised by impedance spectra analysis and modelling in terms of an equivalent circuit consisting of Warburg element, capacitor and resistor, respectively [133,134]. One of these processes dominates under a certain alternating current (ac) frequency, temperature and electrode potential, and determines the performance of an electrochemical system. The electrochemical processes in RTILs, in turn, strongly depend on the charge, size, polarisability and interactions of RTILs ions at the electrode surface at different potentials and temperatures [135]. Thus, a deeper understanding of the chemical structure–interface property dependence should benefit the performance enhancement of known electrochemical systems and reveal novel research directions [3,4]. Obviously, it is of practical and theoretical interest to study the potential and temperature dependences of processes at an electrode immersed in different RTILs.

5.1.2 *Electrical double-layer in* RTILs

In the instance of electrochemistry, RTILs present a challenge, as these electrolytes have high volumetric charge density unlike common dilute aqueous electrolyte solutions. This circumstance is especially important regarding the EDL at the metal | RTIL interface as has been emphasised in an influential article titled "Double-layer in ionic liquids: paradigm change?" in 2007 [21]. The conclusions of this article have strongly influenced the research direction of RTILs in electrochemistry. Firstly, it was shown that there was no deep understanding of the structure and properties of the EDL at the metal | RTIL interface. The EDL in RTILs cannot be described by the mean-field theory as it is possible in case of aqueous electrolytes [21]. Secondly, the absence of theoretical models prevented more sensible applications of the metal | RTIL interfaces in energy storage and conversion devices. In general, these conclusions are still valid.

Let's consider the differential capacitance of the EDL – one of the most important macroscopic properties of all electrochemical systems. Many theories have been developed during the 20th century that successfully describe the dependence of capacitance on potential of an electrode emerged into a dilute electrolyte solution [135]. However, the current understanding of

the capacitive behaviour at metal | RTIL interfaces, characterised by a high concentration of charge carriers, is limited [135]. Most recently such interfaces have attracted much attention due to their high technological potential in various fields of chemistry and physics, and it has become evident that their application at electrified interfaces in energy-storage systems, electrocatalysis, deposition, synthesis, etc. cannot proceed without a deeper understanding of the structure and properties of the EDL. Some aspects and details related to the electrified metal | RTIL interface were addressed by the modified Poisson–Boltzmann theory [21,136–138], density functional theory (DFT) [130–133], mean spherical approximation (MSA) theory [143], and Landau–Ginzburg-type continuum theory [144] as well as molecular dynamic (MD) and Monte-Carlo (MC) simulations [145–153]. Experimental studies at well-defined single crystal electrodes [15,130–132,154–158] and at polycrystalline electrodes [159–166] are inevitable for the verification of the theoretical models including those based on quantum chemical DFT calculations [15,167–170].

In order to describe correctly the experimentally measured differential capacitance dependence on electrode potential and temperature, the compact layer has to be accurately accounted. It must be stressed that in the case of most theories there is an empirical parameter, which describes the closest approach of the adsorbed ions to the electrode surface, i.e. the effective thickness of the compact part of the EDL [21,143,144]. However, the ratio and contributions of the capacitances of the compact (C_H) and the diffuse part in the differential capacitance for RTILs are still unclear. While in the compact layer the ions are adsorbed at the surface, in the diffuse layer the ions move more freely under the influence of thermal motion. By the matter of fact, since the times of Helmholtz, who proposed the first primitive model, and until today, the compact layer has been treated as a parallel plate capacitor neglecting the effects of strong metal–adsorbate and adsorbate–adsorbate interactions as well as their dependence on electrode potential and on temperature. Thus, interpretation of experimental results is incomplete due to the limitations of the theoretical models involved. For instance, Baldelli's interpretation postulating that the EDL is one-layer thick is obviously oversimplified [171]. It only means that the role of the compact layer might be heightened. Alternative statement introduced by Kornyshev [21], that the EDL is more than one-layer thick, is based on the assumption that the differential capacitance might be determined by the diffuse layer capacitance. To sum up, there is a need for new insight explaining and analysing the EDL structure and properties in order to clarify the roles of compact and diffuse layer onto the differential capacitance dependence on electrode potential.

5.1.3 Temperature effect studies by EIS

One of the ways to obtain additional information about the properties of the EDL at the electrode | RTIL interface is by studying the dependence of complex impedance on temperatures. Nowadays, more and more attention is paid to

the C_d,T-dependence in RTILs at different metal and graphite electrodes [131,155,156,159,160,164,165].

Lockett *et al.* [160,165] investigated the EDL properties of glassy carbon electrode in alkylimidazolium-based RTILs: EMImCl, BMImCl, HMImCl. EIS and cyclic voltammetry (CV) were used over wide range of electrode potential and temperature (from 80 to 140℃). It was found that the capacitance, measured at 1000 Hz, increases with temperature. Costa *et al.* [164] measured the effect of temperature on the interface between Hg and alkylimidazolium-based RTILs: EMImTf_2N, BMImTf_2N, HMImTf_2N. The experiment was performed at a temperature range from 30 to 60℃. It was found that the capacitance, measured at 200 Hz, increases with temperature in the whole potential range for all RTILs studied. Previously similar C_d,T-dependence was observed by Silva, Costa *et al.* [159] for the interfaces formed at solid metal (Pt), liquid metal (Hg) and semi-metal glassy carbon (GC) in contact with $BMImPF_6$ within a temperature range from 20 to 75℃.

Most recently Drüschler *et al.* presented their results for the influence of temperature on the differential capacitance for the $Py_{1,4}FAP$ | Au(111) interface for a temperature region from 0 to 90℃ [155]. Differently from other works, it was claimed that the differential capacitance of the electrode | RTIL interface, obtained by the impedance spectra modelling, decreases with increasing temperature. The authors showed that careful analysis of broadband impedance spectra results in a very weak temperature dependence of the high-frequency differential capacitance values. They suggested that capacitance data recorded at a single frequency (as in Ref. [159,160,164,165]) may indicate an apparent strong temperature dependence. The seeming increase of the differential capacitance with increasing temperature, found for single-frequency measurements, is related to the existence of two capacitive processes with different temperature-dependent relaxation times [154,155].

The existence of two or more capacitive processes was described previously in the works of Kolb *et al.* [131,132] and also of Siinor *et al.* [15,130]. For the $BMImPF_6$ | Au(100) [131] and $EMImBF_4$ | Bi(111) [130] interfaces the impedance spectra were carefully modelled using the non-linear least-square method. The high-frequency differential capacitance as well as modelled capacitances were found to increase with increasing temperature. Yet, in the single-frequency measurements much more complex behaviour was found for a Au(111) electrode immersed into $EMImBF_4$, $BMImBF_4$ or $HMImBF_4$ [156]. To sum up, rather different temperature dependences may be found for different RTILs in contact with chemically and crystallographically different electrodes. There is no universal and widely accepted conception-explanation to the dependence of differential capacitance on temperature and electrode potential in a wide temperature region studied.

5.2 Experimental

5.2.1 Experimental procedures

EIS was applied to measure the differential capacitance dependence on the electrode potential (E) and the dependence of complex impedance on the alternating current (ac) frequency (f) at constant electrode potential. The impedance spectra were recorded with Autolab PGSTAT 30 system controlled by the FRA II software. The measuring cells were washed with concentrated sulphuric acid with addition of a small amount of H_2O_2 and heated up to 70℃. C vs. E curves were measured at several fixed values of ac frequency from 1000 to 30 Hz. Impedance spectra were measured within the ac frequency range from 0.1 to 10000 Hz at different fixed electrode potentials. Measurements were performed by moving from negative potentials towards positive potentials and from lower temperatures to higher temperatures. The temperature values within the cell were calibrated and established with an accuracy of ±1℃.

A three-electrode setup was used with a high-surface area Pt mesh counter electrode, a straight Ag wire coated with AgCl (Ag | AgCl) as a reference electrode, and a Cd single crystal established by Mateck and acting as a working electrode. The crystallographic orientation of the Cd(0001) single crystal was determined and controlled by x-ray diffraction method. The final preparation of the electrode was accomplished by electrochemical polishing in an aqueous solution of H_3PO_4, performed before each experiment.

The adsorption kinetics of iodide ions at electrochemically polished Cd(0001) single crystal electrode from aqueous solutions with constant ionic strength $0.1x$ M KI+⅓$0.1(1 - x)$ M K_2SO_4 were studied by EIS (x is the mole fraction of KI in a solution). Measurements were carried out at temperatures of 2, 13, 20, 27, 34℃ in the solutions with constant ionic strength to minimise the influence of the changes in the total solution concentration on the diffusion and adsorption steps. Solutions were prepared from KI and Na_2SO_4 (Aldrich Chemical Company, 99.998%) and Milli Q+ water (ultra purified water using the Milli Q+ purification system, resistance > 18.2 MΩ cm).

$EMImBF_4$ was purchased from Fluka (water content ≤ 200 ppm, electrochemical purity, 99.0%, additionally saturated using argon 99.9999%). All experiments, including handling of the RTIL, were performed inside a glove box in argon (99.999% purity) atmosphere. It is important to note that some impurities often observed in commercial RTILs can strongly alter the surface processes leading to misinterpretations [172]. To avoid the influence of these impurities we have investigated a narrow potential window from −0.5 to −1.0 V, for which cyclic voltammetry does not reveal any noticeable faradaic reactions. All impedance measurements were performed inside glove box (Labmaster sp, LMBraun; O_2 and H_2O concentrations < 1 ppm) at temperature values of 30, 40, 50, 60, 70℃.

5.2.2 Differential, electrical double-layer and absorption capacitances

Differential capacitance (C_d) is a quantity that characterises capacitive properties of an electrode | electrolyte interface:

$$C_d = \frac{\partial \sigma}{\partial E}, \tag{14}$$

where σ is the surface charge density and E is the electrode potential. The capacitance is defined per visible surface area unit. Thus, the differential capacitance of the EDL is an experimentally measurable quantity, which electrode potential dependence is widely used for the EDL structure characterisation. Usually the frequency dependent differential capacitance is measured at a fixed single frequency value. The EIS data modelling allows dividing the differential capacitance into different frequency independent components. For an ideally polarisable system, at frequency $f \to 0$, the differential capacitance is a sum of C_{dl} and C_{ad}, where C_{dl} is the high-frequency, i.e. true electrical double-layer capacitance, which occurs at a constant surface excess (Γ). The absorption capacitance (C_{ad}) appears due to the fact that the surface excess of ions depends on the electrode potential:

$$C_{ad} = (C_0 - C_{dl}) = \left(\frac{\partial \sigma}{\partial \Gamma}\right)_E \left(\frac{\partial \Gamma}{\partial E}\right)_\mu, \tag{15}$$

where low-frequency differential capacitance (C_0) is defined as:

$$C_0 = \left(\frac{\partial \sigma}{\partial E}\right)_{\mu,\Gamma} + \left(\frac{\partial \sigma}{\partial \Gamma}\right)_E \left(\frac{\partial \Gamma}{\partial E}\right)_\mu. \tag{16}$$

The EDL capacitance (C_{dl}) is determined as:

$$C_{dl} = \left(\frac{\partial \sigma}{\partial E}\right)_{\mu,\Gamma}. \tag{17}$$

Fitting of the impedance spectra with the equivalent circuit (Fig. 13) was performed for both interfaces under study: Cd(0001) | $EMImBF_4$ and Cd(0001) | $0.1x$ M KI + ⅓×0.1(1 – x) M Na_2SO_4. The expression for the modelled capacitance in terms of C_{dl} and C_{ad} is:

$$C(j\omega) = C_{dl} + \frac{1}{j\omega R_{ct}} + \frac{C_{ad}}{1 + j\omega Z_W C_{ad}}, \tag{18}$$

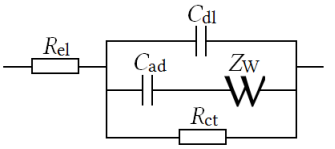

Figure 13. Modified Frumkin–Melic-Gaikazyan equivalent circuit, where: R_{el} – electrolyte resistance, C_{dl} – electrical double-layer capacitance, C_{ad} – adsorption capacitance, R_{ct} – partial charge transfer resistance, Z_w – Warburg diffusion impedance.

5.3 Experimental results

5.3.1 Cyclic voltammetry

CV method was used to verify the electrode potential region free form faradaic reactions, purity of the ionic liquid and reproducibility of the system. In Fig. 14 three cyclic voltammograms for Cd(0001) electrode in contact with $EMImBF_4$, measured within different potential cycling regions, are shown. Significant cathodic and anodic faradaic currents rise beyond −1.2 V and −0.4 V (CV1 and CV2), respectively. At anodic potentials dissolution of Cd(0001) electrode takes place, which is visually observable. At more cathodic potentials (E < −1.1 V) a reaction of residual water and O_2 occurs. Therefore, we limited our EIS measurements to a narrow potential region from −1.0 V to −0.5 V (CV3), to avoid influence of these parasitic faradaic processes onto impedance spectra.

5.3.2 Nyquist (Z'', Z') and Bode (δ, f) plots

Figure 15a shows (Z'', Z') Nyquist dependencies measured at fixed temperature (T = 30°C) and different electrode potentials. The impedance spectra are significantly influenced by occurrence of parasitic faradaic processes, which we modelled by parallel charge transfer process with a resistance (R_{ct}) in the equivalent circuit (Fig. 13). The value of R_{ct} depends on the preparation procedure of experiment and is most probably sensitive to the concentration of residual water and other electrochemically active contaminants in the RTIL. In spite of deflection of all experimental results from each other at low frequencies (f < 20 Hz), it is seen that the curves for all experiments coincide at f > 20 Hz (Fig. 15a). Consequently the fast capacitive process of EDL formation (C_{dl}) is reproduced with a very good accuracy from experiment to experiment. Figure 15b shows complex admittance plots at different temperatures and at fixed potential (E = −0.8 V), where Y'' is the imaginary and Y' is the real parts of admittance, respectively [133]. The deviation of the measured admittance from the ideal semicircle (dotted lines) is seen, which indicates the significant effect of mass transfer process. The latter process was modelled by Warburg impedance (Fig. 13).

The proportion of limiting stages determining the speed of the total process can be assessed by the phase angle (δ) dependence on the ac frequency (f) (Figs. 16 and 17). At high ac frequencies, the fast EDL charging occurs. Herewith, this process is hindered by the electrolyte resistance. At low ac frequencies, on the other hand, the adsorption is hindered by mass transfer (diffusion) and charge transfer processes. Figures 16 and 17 show that at very low ac frequencies the charge transfer is the dominating process as $\delta \rightarrow 0°$. In low-frequency areas, the δ,f-curves demonstrate the dependence of δ on temperature within the whole potential range. The higher the temperature, the more the speed is determined by charge transfer process rate. Such disper-

sion is clearly seen in the instance of more negative potentials (Figs. 17a and 17b). At potentials $E = -0.5$ V and $E = -0.6$ V, the dependence of δ on temperature is within the experimental error. At 10–100 Hz, for all systems nearly ideal adsorptive behaviour is observed ($\delta \leq -80°$), herewith the lower the temperature, the higher the absolute values of δ (Figs. 17a and 17b).

5.3.3 Capacitance

The adsorption capacitance and the EDL capacitance values (Fig. 18) were obtained by fitting the measured impedance spectra using the equivalent circuit (Fig. 13) and applying non-linear least-square fitting method. Details are provided in Ref. [16]. The EDL capacitance for Cd(0001) | $EMImBF_4$ interface has a maximum near $E = -0.8$ V, where the PZC is most likely located (Fig. 18b). In contrast, C_d has a very wide minima at this potential (Fig. 18a). This finding supplement the statement of Drüschler *et al.* [155] that single-frequency experiments may lead to artefacts not only in the temperature, but also in the potential dependence of the differential capacitance. The fitting results for C_{ad} values do not correspond to the measured C_d values at low frequencies due to disturbance of impedance spectra by mass and charge transfer processes. To obtain the frequency independent capacitance values, fitting methods of impedance spectra must be applied. For this reason, the very interesting results gained by Alam *et al.* [156] for Au(111) | $EMImBF_4$ using single-frequency measurements have to be taken with a great caution.

Much better agreement between C_d and C_{dl} values is seen in the results for Cd(0001) | $0.1x$ M KI + ⅓×0.1$(1 - x)$ M Na_2SO_4 (Fig. 18d and 18e). Although the same reference electrode is used in the RTIL and aqueous solutions, the measured electrode potential scales are different due to different solubility of AgCl in these media. The PZC in surface inactive electrolyte solution is located at $E = -0.95$ V [35]. Hence, I^- anion already adsorbs at negative surface charge densities. We may speculate that specific adsorption, i.e. accomplished by the formation of covalent binding to the surface, begins at $E > -1.0$ V, where the adsorption capacitance dependence on temperature appears. In the range of electrode potentials from −1.4 V to −1.0 V the iodide ion enters into the EDL compact layer, as may be judged comparing the results to the C_{dl} measured for Cd(0001) | ⅓×0.1 M Na_2SO_4 (Fig. 18e) [20].

The most remarkable difference of the results for different electrolytes is that the EDL capacitance is decreasing in aqueous solutions with the rise of temperature, while it is increasing in RTILs. Herewith the adsorption capacitance increases for both electrolytes with increasing temperature (Fig. 18).

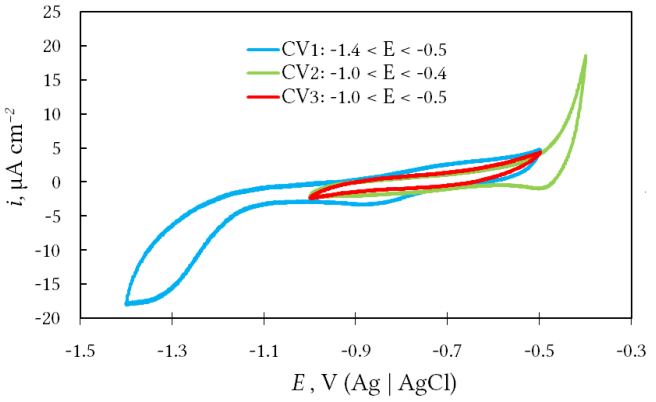

Figure 14. Cyclic voltammograms for Cd(0001) in $EMImBF_4$ at scan rate of $\nu = 20\ mVs^{-1}$. First scan starting from −1.0 V in cathodic direction is shown for three different potential cycling regions (indicated in the figure).

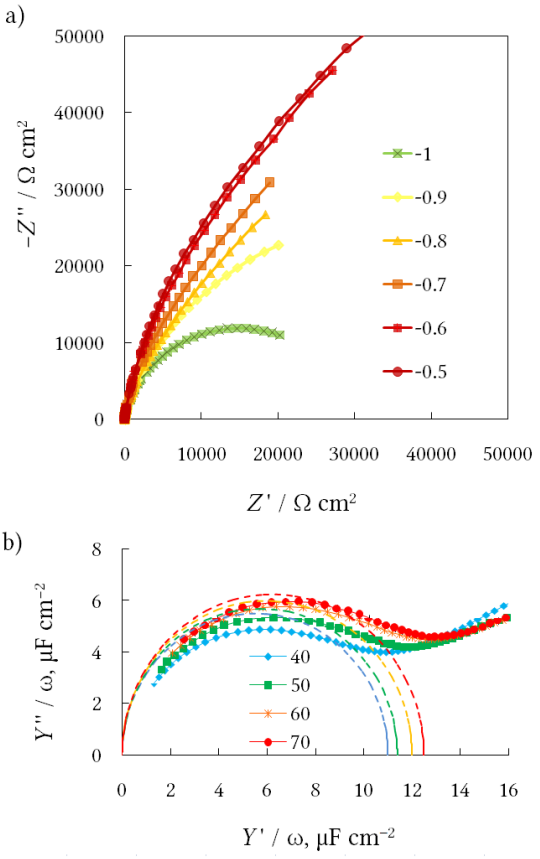

Figure 15. a) Z'',Z'-dependencies (T = 30℃) at different electrode potentials (indicated in the figure). b) Y''/ω,Y'/ω-dependencies (E = −0.8 V) at different temperatures (indicated in the figure).

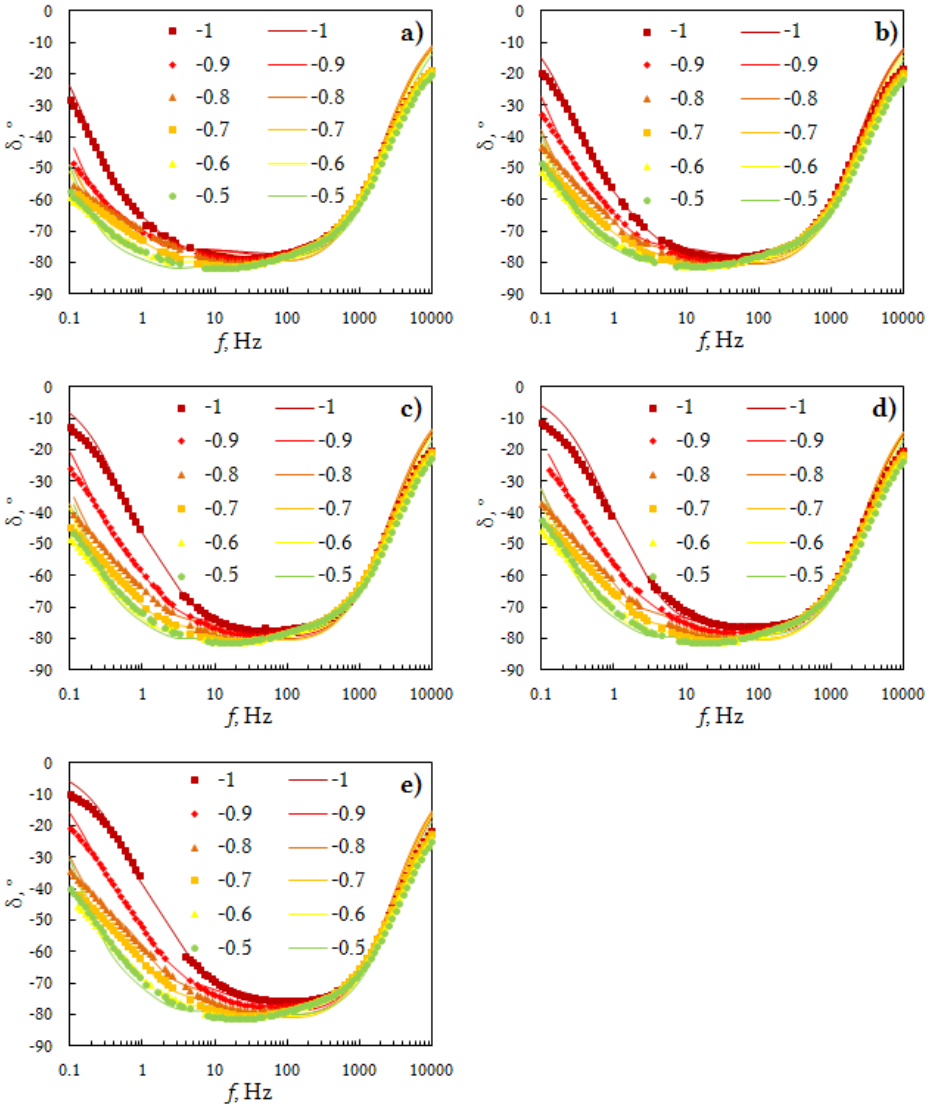

Figure 16. Phase angle dependence on frequency at different potentials (indicated in the figure) and at various fixed temperatures (℃): a) 30; b) 40; c) 50; d) 60; e) 70.

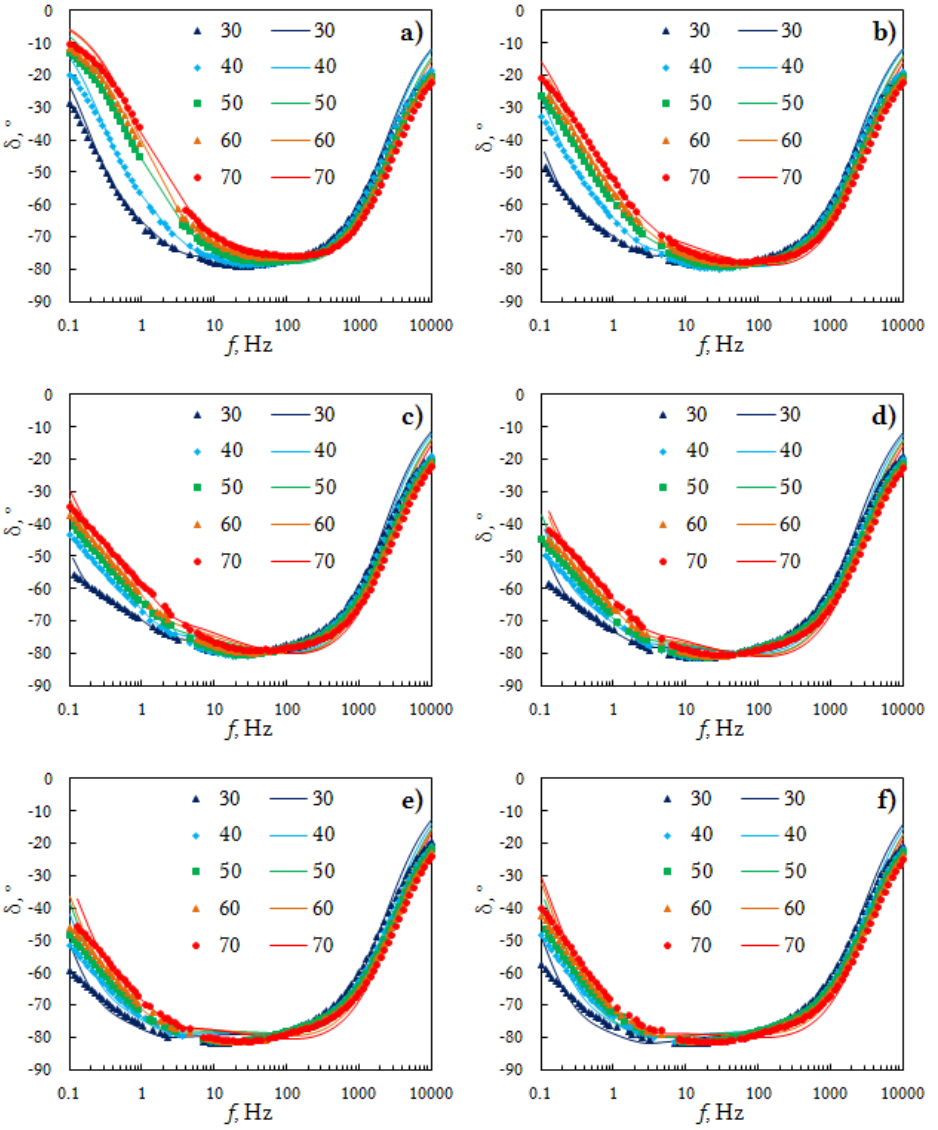

Figure 17. Phase angle dependence on frequency at various fixed potentials : a) −1.0; b) −0.9; c) −0.8; d) −0.7; e) −0.6; f) −0.5 V vs. Ag | AgCl, and different temperatures (indicated in the figure).

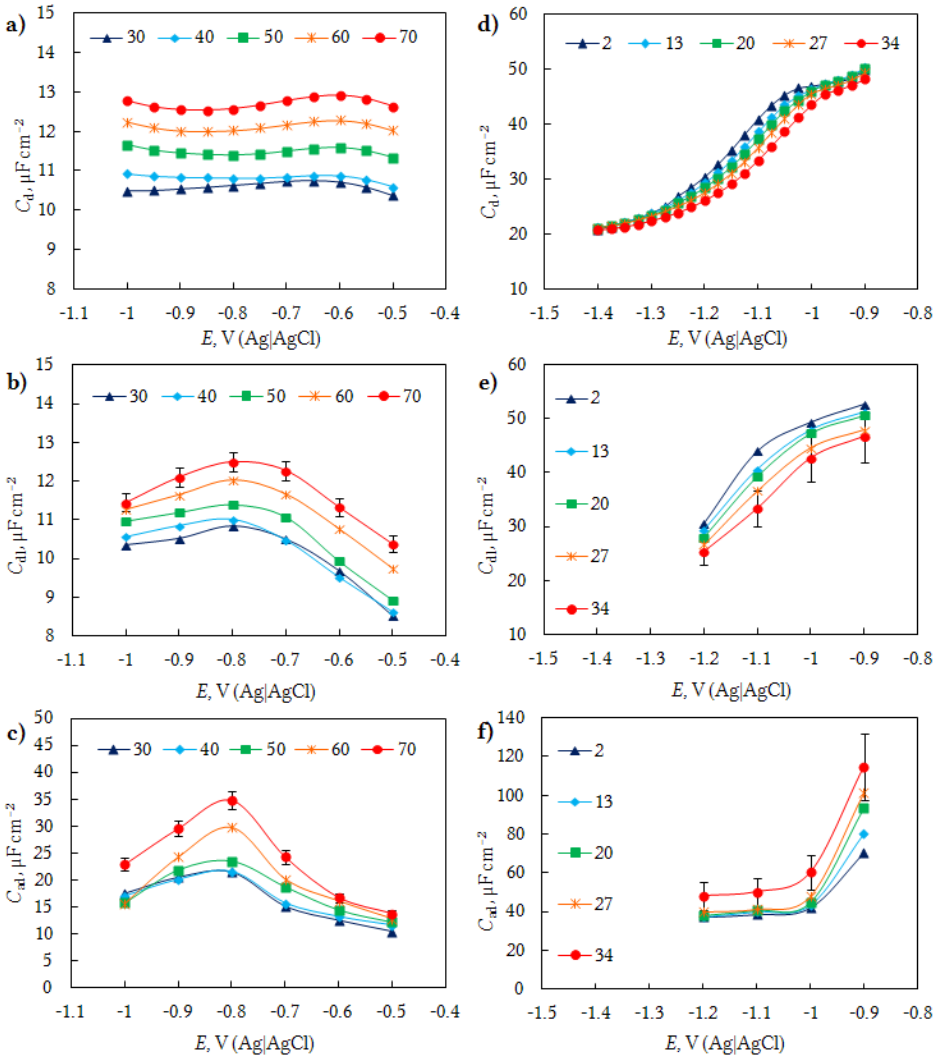

Figure 18. Dependences of a) differential capacitance (C_d) (f = 201 Hz) b) high-frequency or EDL capacitance (C_{dl}) and c) adsorption capacitance (C_{ad}) on the Cd(0001) electrode potential in $EMImBF_4$ at different temperatures (indicated in the figure). Values for C_{dl} and C_{ad} have been obtained by impedance spectra modelling.

6. Discussions

Simple explanation for the C_{dl},T-dependence for aqueous solutions can be given on the basis of the model presented in section 4.3.2. Without additional DFT calculations, i.e. for a very rough qualitative demonstration, we adjusted two parameters of the model to mimic the experimental results. At first, to obtained the C_{dl},σ-dependence, shown in Fig. 19, we used the value of 0.08 nm for I^- position (near the Bi surface) in addition to the calculated z_{avg} value (section 4.3.3). This effective value indicates an approach of the anions and their penetration to the interfacial H_2O layer. Secondly, we used Gibbs adsorption values for I^- adsorption at the Bi(111) surface from Ref. [33] to introduce iodide–image-charge dipole formation energy into the dipole lattice model. Such a choice is justified by a similarity of the iodide adsorption at Bi(111) and Cd(0001) electrodes described in our previous work [20]. We used a value of the dipole moment, created by the adsorbed anion and its image charge in the metal, comparable to the value of effective dipole moment estimated by our colleges in thermodynamic studies of Bi(111) and Bi(001) | aqueous electrolyte interfaces [29,31,33]. As a first approximation, the obtained theoretical C_H,σ-dependence is consistent with the experiment. Thus, we may state, that the origin of the EDL capacitance dependence on temperature (Fig. 18) in aqueous solution is lying in the EDL compact layer. Thermal distortion affects the dipole lattice of H_2O and adsorbed I^- distance causing the decrease in the EDL capacitance with increasing temperature. This effect facilitates the specific adsorption of I^-, giving rise to the adsorption capacitance increases with increasing temperature.

The effect of increasing temperature is expressed differently for the $EMImBF_4$ | Cd(0001) interface: C_d and C_{dl} increase with increasing temperature in the whole potential range (Figs. 18a and 18b). Similar temperature dependence of C_d has also been observed by Silva *et al.* [159], Lockett *et al.* and Costa *et al.* [164]. Small modelled C_{dl} increase was also observed by Gnahm *et al.* [131] and Siinor *et al.* [129]. Such C_{dl},T-dependence (Fig. 18b) can be explained by modern phenomenological models and by applying recent theoretical descriptions of the EDL.

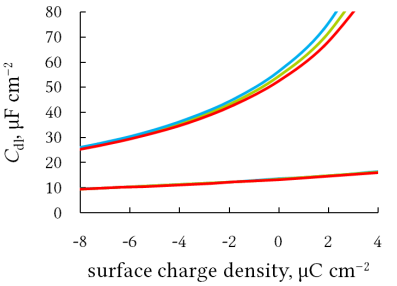

Figure 19. Modelled C_{dl},T-dependence. Lower values correspond to an inactive electrolyte solution. Higher values refer to the modelled iodide adsorption. Blue, green and red lines correspond to 2, 20 and 34℃, respectively.

6.1.1 *Models of the* EDL *structure at electrode* | RTIL *interface*

Since 2007 a number of *in situ* scanning tunneling microscopy (STM) studies have revealed the existence of ordered structures at charged electrodes [131,173–176]. Some years later it was demonstrated using *in situ* atomic force microscopy (AFM) that the RTIL structure represents a well-ordered region near the electrode surface [176–179]. An exaggerated representation of the interface between metal and RTIL is shown in Figure 20.

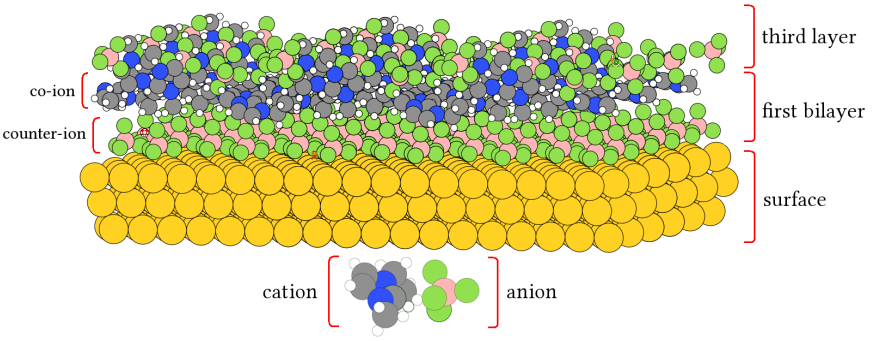

Figure 20. Model of the RTIL structure near the the electrode surface.

The first bilayer adjacent to the solid surface is considerably denser than the others [180,181]. It consists of cations and anions forming two layers: one layer of counter-ions with charge opposite by sign to the charge of electrodes and another of co-ions. Counter-ions charge density overscreens the co-ions charge density, consequently co-ion repulsion from the charged surface is less pronounced than it might be expected. Second layer and consequent bilayers have similar divisions in counter and co-ion layers, however, with less expressed structural ordering. Also the magnitude of the charge densities of counter-ions and co-ions (relative to the charge densities of cations and anions in the bulk) decreases at a distance from the electrode. Specific structure of the RTIL provides excellent electrostatic screening at a distance of 1–2 nm [182], i.e. at distances smaller than in common aqueous electrolyte solutions (taking into account the diffuse layer thickness). The depth of the interfacial structure propagation into the bulk depends on the chemical structure of the RTIL, electrode potential, temperature and probably on the concentration of residual impurities [176]. The relative magnitude of an ion-layer charge density at the RTIL | electrode interface decreases with increasing temperature as it was shown in recent MD simulations [147,151,152]. MD studies confirm that the electrode | RTIL interface structure represents a well-ordered region, in which cations and anions form alternating layers. Dou *et al.* [152] found in their MD experiment for graphite | $BMImPF_6$ interface that the peaks related to the well-ordered surface structure become weaker and the third and fourth layers even disappeared with the temperature rise from 400 to 800 K [152] The same interface was studied by Kislenko *et al.*

[147] in a lower temperature range from 300 K to 400 K. In general MD, AFM and EIS studies supplement each other hinting to a glass-like structure of the EDL compac layer at low temperatures and high voltages revealing the slowness of the mass transfer and adsorption of ions near the electrode surface. These processes become faster or even comparable to the dynamics of the bulk with increasing temperature.

6.1.2 *Theories of* EDL *at electrode* | RTIL *interface*

Division of the EDL at metal | RTIL interface into Helmholtz and diffuse layer is unjustified due to the multilayer interface structure. The innermost layer, mentioned and discussed above, obviously gives highest impact to the capacitance of the EDL:

$$C = \frac{\varepsilon \varepsilon_0}{d_0}, \tag{19}$$

where, at zeroth approximation, d_0 is the distance of closest approach of ions to the surface, i.e. the distance from the electrode surface to the centre of counter-ions layer; ε is relative dielectric constant. In this form the Helmholtz layer capacitance approximation appears in several modern theories [21,144] and is constantly recalled to explain the experimental results obtained for the electrode | RTIL interface [160,162,163,171]. Notice that Eq. 19 resembles Eq. 10, where effective parameter ε is described in terms of interplay of metal and solvent layer capacitances (section 4.3.2). In MD simulations the distance changes only slightly upon temperature changes [147,152]. Thus, the dielectric constant should increase with increasing temperature, as thermally distorted ions have more degrees of freedom, until it reaches the value characteristic for the bulk dielectric constant of RTIL. On the other hand, according to Kirkwood's formula [183], the bulk dielectric constant decreases with increasing temperature. For this reason the capacitance can increase with increase of temperature until some critical temperature, at which the value of the compact layer dielectric constant would reach the bulk value.

Differently from Eq. 19, in MSA theory [143] the differential capacitance is expressed as:

$$C = \frac{\varepsilon \varepsilon_0}{2\pi} \gamma, \tag{20}$$

where γ is a renormalised screening constant:

$$\gamma = \frac{d_0 \sqrt{1+\kappa} - 2}{2 d_0} \sim \kappa. \tag{21}$$

Here κ is the Debye screening parameter. The MSA theory predicts a decrease of the capacitance as $\kappa \sim T^{-1/2}$ (this result comes from Taylor series expansion of Eq. 21) [184]. However, when an association of ions in the EDL compact

layer is taken into account via mass-action law (MAL), the capacitance increase can take place at relatively low temperatures. In the combined MSA-MAL theory the RTIL is considered to be a mixture of free ions and complex ionic aggregates. This leads to the corrected renormalised screening constant:

$$\gamma = \frac{a\sqrt{1+\kappa\sqrt{\alpha}}-2}{2a} \sim \kappa\sqrt{\alpha}. \tag{22}$$

At high temperatures, $\alpha \longrightarrow 1$, and for this reason a classical behaviour of capacitance on temperature is expected for electrode | RTIL interface [184]. At lower temperatures, $\alpha \longrightarrow 0$, which implies a change in the temperature dependence. Qualitatively this theory predicts behaviour observed in this research (Fig. 18b), if the main assumption of the ionic association is clearly justified. To constitute the need for accounting the ion-pair formation, firstly, we have to keep in mind that ρ_0 is related to the surface excess of ions. Secondly, from a structural point of view, the directionality of the ion-pair by the H-bond formation is known to result in fast and slow dynamics in RTIL bulk [185]. Due to a correlation of ions, at least in imidazolium based RTILs, at a given moment most ions can be grouped in pairs, although, the hydrogen bonds are too weak to hold these pairs together for a long time [186]. The correlation is distorted by high temperature giving more degrees of freedom to the interfacial structure and releasing free ions.

Two different interpretations presented provide similar qualitative description. The first approximation mainly considers the influence and change of the relative permittivity, the second assumes only behaviour of the effective distance in terms of renormalised screening constant.

A generalised approach was recently proposed by Feng *et al.* [187] in a framework of "counter-charge layer in generalised solvents" model. Within this approach, the effective quantity ε / d is expressed as:

$$C = \frac{\varepsilon\varepsilon_0}{d} = \frac{\varepsilon_0}{d_0 \sum_{i=1}^{N} (-1)^i \gamma_i \Delta_i}, \tag{23}$$

where $\gamma_i \Delta_i$ values are calculated numerically based on data obtained from MD simulation and have the meaning of screening constant multiplied by the average distance between the counter-ion and co-ion of the i-th layer. $\gamma_i \Delta_i$ decreases with increase of layer index i.

The dielectric screening inside EDL is mainly controlled by a few innermost EDL layers [187]. If there were only one layer, the capacitance would be equal to ε_0/d_0, as for the classical Helmholtz model (Eq. 19) with $\varepsilon = 1$. An addition of a second layer would decrease the distance d and thence increase the capacitance to the value calculated as: $\varepsilon_0/(d_0 - \gamma_1 \Delta_1)$. However, an addition of a third layer would decrease the value: $\varepsilon_0/(d_0 - \gamma_1 \Delta_1 + \gamma_2 \Delta_2)$. In a reverse order, under thermal distortion, the disappearance of the third layer would result in capacitance increase until only two layers remain, and then disappearance of the

second layer would lead to the capacitance decrease.

Three explanations, applicable for electrode | RTIL interface, are based on: 1) phenomenological theory, 2) MSA-MAL approximation and 3) MD simulations, respectively. They are in qualitative agreement with a vast number of experimental, theoretical and computational studies, as well as with EIS data collected during this study (Figs. 16, 17 and 18). Therefore, it can be concluded that the increase in the observed capacitance values is related to the changes in the interfacial structure and properties (d, ε) of electrode | RTIL interface caused by an increase of temperature. This phenomenon results from a distortion of the electrostatic interactions between the ions by thermal excitation, and may be described as possible gradual dissolution of the EDL layered structure. The described possibility of the EDL capacitance decrease was confirmed in the works of Drüschler *et al.* [155] and Siinor *et al.* [129], as well as in high-temperature MD simulations [188].

7. Conclusions

Electrochemical Impedance spectroscopy and cyclic voltammetry methods have been applied for characterising the processes at the interface between single crystal Cd(0001) electrode and 1-ethyl-3-methylimidazolium tetrafluoroborate ($EMImFB_4$) as well as adsorption of I^- anion on an electrochemically polished Cd(0001) electrode from aqueous electrolyte solutions.

In both cases the impedance spectra were fitted using the modified Frumkin–Melik-Gaikazyan model, which gives better fitting results compared to alternative equivalent circuits. This indicates that the adsorption process(es) in aqueous solution and room temperature ionic liquid follow similar patterns.

However, the modelled high-frequency differential capacitances show different dependence on temperature. In the case of I^- anion the decrease of the differential capacitance with increasing temperature can be qualitatively explained with the help of the dipole lattice model. Coupled results of Density Functional Theory (DFT) based calculations and statistical approach indicate that the repulsion between iodide–image charge dipoles weakens with the rise of temperature, leading to a decrease of the high-frequency capacitance and also to an increase in the adsorption capacitance. Thus, the EDL compact layer properties determine the differential capacitance behaviour.

In contrast, the high-frequency capacitance for Cd(0001) | $EMImBF_4$ increases with increasing temperature. The presented theoretical explanations lead to the conclusion that the differential capacitance is determined by the multilayered structure of the EDL, which gradually "dissolves" with increasing temperature.

Current experimental research allows us to compare the results collected at Cd(0001) electrode to those measured at Au(111) [156], Bi(111) [15,189] and glassy carbon [190] electrodes immersed in $EMImBF_4$. The capacitance values for these three metals are almost equal and higher than for glassy carbon electrode. The differential capacitance dependence on the electrode potential differs for Bi(111) | $EMImBF_4$ and Cd(0001) | $EMImBF_4$ interfaces. For this reason both systems are interesting objects for further DFT based studies.

8. References

[1] B. Kirchner, Ionic Liquids, Springer-Verlag, Berlin, 2010.
[2] M. Galiński, A. Lewandowski, I. Stępniak, Electrochim. Acta 51 (2006) 5567.
[3] M. Armand, F. Endres, D.R. MacFarlane, H. Ohno, B. Scrosati, Nat. Mater. 8 (2009) 621.
[4] H. Liu, Y. Liu, J. Li, Phys. Chem. Chem. Phys. 12 (2010) 1685.
[5] A. Lewandowski, M. Galinski, J. Power Sour. 173 (2007) 822.
[6] M. Mastragostino, F. Soavi, in: Encyclopedia of Electrochemical Power Sources, Elsevier, Amsterdam, 2009.
[7] T. Torimoto, T. Tsuda, K. Okazaki, S. Kuwabata, Adv. Mat. 22 (2010) 1196.
[8] J. Schaefer, Y. Lu, S. Moganty, P. Agarwal, N. Jayaprakash, L. Archer, Appl. Nanosci. 2 (2012) 91.
[9] S. Passerini, W.A. Henderson, in: Encyclopedia of Electrochemical Power Sources, Elsevier, Amsterdam, 2009.
[10] B. Li, L. Wang, B. Kang, P. Wang, Y. Qiu, Sol. Energ. Mat. Sol. C. 90 (2006) 549.
[11] H. Kurig, A. Janes, E. Lust, J. Electrochem. Soc. 157 (2010) A272.
[12] H. Kurig, M. Vestli, A. Janes, E. Lust, Electrochem. Solid-State Lett. 14 (2011) A120.
[13] V. Palmre, D. Brandell, U. Mäeorg, J. Torop, O. Volobujeva, A. Punning, U. Johanson, M. Kruusmaa, A. Aabloo, Smart Mat. St. 18 (2009) 095028.
[14] V. Palmre, E. Lust, A. Jänes, M. Koel, A.L. Peikolainen, J. Torop, U. Johanson, A. Aabloo, J. Mater. Chem. 21 (2011) 2577–2583.
[15] L. Siinor, C. Siimenson, V. Ivaništšev, K. Lust, E. Lust, J. Electroanal. Chem. 668 (2012) 30.
[16] V. Ivaništšev, A. Ruzanov, K. Lust, E. Lust, In preparation.
[17] V. Ivaništšev, R. Nazmutdinov, E. Lust, in:, The 61st Annual Meeting of the International Society of Electrochemistry, Nice, France, 2010, p. 199.
[18] V. Ivanistsev, R.R. Nazmutdinov, E. Lust, Submitted to Surf. Sci.
[19] V. Ivanistsev, R.R. Nazmutdinov, E. Lust, Surf. Sci. 604 (2010) 1919.
[20] L. Siinor, V. Ivaništšev, K. Lust, E. Lust, J. Solid State Chem. 14 (2010) 555.
[21] A.A. Kornyshev, J. Phys. Chem. B 111 (2007) 5545.
[22] E. Lust, in: E. Gileadi, M. Urbakh, A.J. Bard, M. Stratmann (eds) Encyclopedia of Electrochemistry, Vol. 1, Wiley-VCH, Weinheim, 2002.
[23] S. Trasatti, E. Lust, in: R.E. White, B.E. Conway, J.O'M. Bockris (eds) Modern Aspects of Electrochemistry, Vol. 33, Kluwer/Plenum, New York, 1999.
[24] O.M. Magnussen, Chem. Rev. 102 (2002) 679.
[25] V.V. Emets, B.B. Damaskin, Russ. J. Electrochem. 45 (2009) 45.

[26] A.A. Kornyshev, E. Spohr, M.A. Vorotyntsev, in: E. Gileadi, M. Urbakh, A.J. Bard, M. Stratmann (eds)
Encyclopedia of Electrochemistry, Vol. 1, Wiley-VCH, Weinheim, 2002.
[27] G. Horányi, G.G. Láng, J. Colloid Interface Sci. 296 (2006) 1.
[28] W. Schmickler, Ann. Rep. Sect. C 95 (1999) 117.
[29] K. Lust, M. Väärtnõu, E. Lust, J. Electroanal. Chem 532 (2002) 303.
[30] E. Lust, A. Jänes, K. Lust, M. Väärtnõu, Electrochim. Acta 42 (1997) 771.
[31] K. Lust, M. Väärtnõu, E. Lust, Electrochim. Acta 45 (2000) 3543.
[32] E. Lust, A. Jänes, K. Lust, V. Sammelselg, P. Miidla,
Electrochim. Acta 42 (1997) 2861.
[33] K. Lust, E. Lust, J. Electroanal. Chem. 552 (2003) 129.
[34] E. Lust, A. Jänes, K. Lust, P. Miidla, J. Electroanal. Chem 413 (1996) 175.
[35] E. Lust, A. Jänes, K. Lust, J. Erlich, Russ. J. Electrochem. 32 (1996) 552.
[36] V.V. Emets, B.B. Damaskin, Russ. J. Electrochem. 40 (2004) 1066.
[37] V.V. Emets, B.B. Damaskin, Russ. J. Electrochem. 40 (2004) 56.
[38] M.A. Henderson, Surf. Sci. Reports 46 (2002) 1.
[39] A.D. Becke, Phys. Rev. A 38 (1988) 3098.
[40] C. Lee, W. Yang, R.G. Parr, Phys. Rev. B 37 (1988) 785.
[41] P.J. Hay, W.R. Wadt, The Journal of Chemical Physics 82 (1985) 270.
[42] Gaussian 03, Revision C.02, M. J. Frisch, G. W. Trucks, H. B. Schlegel, G. E. Scuseria, M. A. Robb, J. R. Cheeseman, J. A. Montgomery, Jr., T. Vreven, K. N. Kudin, J. C. Burant, J. M. Millam, S. S. Iyengar, J. Tomasi, V. Barone, B. Mennucci, M. Cossi, G. Scalmani, N. Rega, G. A. Petersson, H. Nakatsuji, M. Hada, M. Ehara, K. Toyota, R. Fukuda, J. Hasegawa, M. Ishida, T. Nakajima, Y. Honda, O. Kitao, H. Nakai, M. Klene, X. Li, J. E. Knox, H. P. Hratchian, J. B. Cross, V. Bakken, C. Adamo, J. Jaramillo, R. Gomperts, R. E. Stratmann, O. Yazyev, A. J. Austin, R. Cammi, C. Pomelli, J. W. Ochterski, P. Y. Ayala, K. Morokuma, G. A. Voth, P. Salvador, J. J. Dannenberg, V. G. Zakrzewski, S. Dapprich, A. D. Daniels, M. C. Strain, O. Farkas, D. K. Malick, A. D. Rabuck, K. Raghavachari, J. B. Foresman, J. V. Ortiz, Q. Cui, A. G. Baboul, S. Clifford, J. Cioslowski, B. B. Stefanov, G. Liu, A. Liashenko, P. Piskorz, I. Komaromi, R. L. Martin, D. J. Fox, T. Keith, M. A. Al-Laham, C. Y. Peng, A. Nanayakkara, M. Challacombe, P. M. W. Gill, B. Johnson, W. Chen, M. W. Wong, C. Gonzalez, and J. A. Pople, Gaussian, Inc., Wallingford CT, 2004.
[43] Gaussian 09, Revision A.1, M. J. Frisch, G. W. Trucks, H. B. Schlegel, G. E. Scuseria, M. A. Robb, J. R. Cheeseman, G. Scalmani, V. Barone, B. Mennucci, G. A. Petersson, H. Nakatsuji, M. Caricato, X. Li, H. P. Hratchian, A. F. Izmaylov, J. Bloino, G. Zheng, J. L. Sonnenberg, M. Hada, M. Ehara, K. Toyota, R. Fukuda, J. Hasegawa, M. Ishida, T. Nakajima, Y. Honda, O. Kitao, H. Nakai, T. Vreven, J. A. Montgomery, Jr., J. E. Peralta, F. Ogliaro, M. Bearpark, J. J. Heyd, E. Brothers, K. N. Kudin, V. N. Staroverov, R. Kobayashi, J. Normand,

K. Raghavachari, A. Rendell, J. C. Burant, S. S. Iyengar, J. Tomasi,
M. Cossi, N. Rega, J. M. Millam, M. Klene, J. E. Knox, J. B. Cross,
V. Bakken, C. Adamo, J. Jaramillo, R. Gomperts, R. E. Stratmann,
O. Yazyev, A. J. Austin, R. Cammi, C. Pomelli, J. W. Ochterski,
R. L. Martin, K. Morokuma, V. G. Zakrzewski, G. A. Voth, P. Salvador,
J. J. Dannenberg, S. Dapprich, A. D. Daniels, Ö. Farkas, J. B. Foresman,
J. V. Ortiz, J. Cioslowski, and D. J. Fox,
Gaussian, Inc., Wallingford CT, 2009.
[44] C.E. Check, T.O. Faust, J.M. Bailey, B.J. Wright, T.M. Gilbert,
L.S. Sunderlin, J. Phys. Chem. A 105 (2001) 8111.
[45] A. Hölwarth, M. Böhme, S. Dapprich, A.W. Ehlers, A. Gobbi, V. Jonas,
K.F. Köhler, R. Stegmann, A. Veldkamp, G. Frenking,
Chem. Phys. Lett. 208 (1993) 237.
[46] W. Schmickler, J. Electroanal. Chem. 149 (1983) 15.
[47] W.R. Fawcett, J. Chem. Phys. 93 (1990) 6813.
[48] B.L. Maschhoff, J.P. Cowin, J. Chem. Phys. 101 (1994) 8138.
[49] R. Saradha, M.V. Sangaranarayanan, Langmuir 13 (1997) 5470.
[50] R. Saradha, M.V. Sangaranarayanan, J. Phys. Chem. B 102 (1998) 5099.
[51] R.R. Nazmutdinov, T.T. Zinkicheva, M.S. Shapnik,
Russ. J. Electrochem. 35 (1999) 1249.
[52] R.R. Nazmutdinov, M. Probst, K. Heinzinger,
J. Electroanal. Chem. 369 (1994) 227.
[53] J. Ireta, J. Neugebauer, M. Scheffler, J. Phys. Chem. A 108 (2004) 5692.
[54] R. Ludwig, Angew. Chem. Int. Edit. 40 (2001) 1808.
[55] B. Kolb, T. Thonhauser, Phys. Rev. B 84 (2011) 045116.
[56] A.K. Kelkkanen, B.I. Lundqvist, J.K. Nørskov,
J. Chem. Phys. 131 (2009) 046102.
[57] J.-D. Chai, M. Head-Gordon, Phys. Chem. Chem. Phys. 10 (2008) 6615.
[58] T. Yanai, D.P. Tew, N.C. Handy, Chem. Phys. Lett. 393 (2004) 51.
[59] S. Wei, H. Oyanagi, W. Liu, T. Hu, S. Yin, G. Bian,
J. Non-Cryst. Solids 275 (2000) 160.
[60] N. Gaston, B. Paulus, K. Rosciszewski, P. Schwerdtfeger, H. Stoll,
Phys. Rev. B 74 (2006) 094102.
[61] D.R. Lide (ed), CRC Handbook of Chemistry and Physics,
CRC Press/Taylor and Francis, 2008.
[62] P. Hofmann, Prog. Surf. Sci. 81 (2006) 191.
[63] A.B. Anderson, N.M. Neshev, R.A. Sidik, P. Shiller,
Electrochim. Acta 47 (2002) 2999.
[64] L. Árnadóttir, E.M. Stuve, H. Jónsson, Surf. Sci. 604 (2010) 1978.
[65] R. Blanco, J.M. Orts, Electrochim. Acta 53 (2008) 7796.
[66] J. Carrasco, A. Michaelides, M. Scheffler,
J. Chem. Phys. 130 (2009) 184707.
[67] M.L. Grecea, E.H.G. Backus, B. Riedmuller, A. Eichler, A.W. Kleyn,
M. Bonn, J. Phys. Chem. B 108 (2004) 12575.

[68] M. Ito, M. Nakamura, Faraday Discuss. 121 (2002) 71.
[69] G.S. Karlberg, Phys. Rev. B 74 (2006) 153414.
[70] T. Ohwaki, K. Yamashita, J. Electroanal. Chem 504 (2001) 71.
[71] T. Ohwaki, K. Kamegai, K. Yamashita,
Bull. Chem. Soc. Jap. 74 (2001) 1021.
[72] M. Otani, I. Hamada, O. Sugino, Y. Morikawa, Y. Okamoto, T. Ikeshoji,
Phys. Chem. Chem. Phys. 10 (2008) 3609.
[73] E. Skúlason, G.S. Karlberg, J. Rossmeisl, T. Bligaard, J. Greeley,
H. Jónsson, J.K. Nørskov, Phys. Chem. Chem. Phys. 9 (2007) 3241.
[74] C.D. Taylor, M. Neurock, Curr. Opin. Solid St. M. 9 (2005) 49.
[75] Y. Cao, Z.X. Chen, Surf. Sci. 600 (2006) 4572.
[76] J.S. Filhol, M.L. Bocquet, Chem. Phys. Lett. 438 (2007) 203.
[77] J. Li, S. Zhu, Y. Li, F. Wang, Phys. Rev. B 76 (2007) 235433.
[78] J. Li, S. Zhu, Y. Li, F. Wang, J. Am. Chem. Soc. 130 (2008) 11140.
[79] J. Li, S. Zhu, H. Li, E.E. Oguzie, Y. Li, F. Wang,
J. Phys. Chem. C 113 (2009) 1931.
[80] A. Roudgar, A. Groß, Chem. Phys. Lett. 409 (2005) 157.
[81] A. Ignaczak, J. Gomes, J. Electroanal. Chem. 420 (1997) 209.
[82] S. Izvekov, A. Mazzolo, K. VanOpdorp, G.A. Voth,
J. Chem. Phys. 114 (2001) 3248.
[83] M.T.M. Koper, R.A. van Santen, J. Electroanal. Chem 472 (1999) 126.
[84] I. Nechaev, A. Vvedenskii, Prot. Met. Phys. Chem. Surf. 45 (2009) 391.
[85] J. Ren, S. Meng, Phys. Rev. B 77 (2008) 54110.
[86] H. Ruuska, T.A. Pakkanen, R.L. Rowley,
J. Phys. Chem. B 108 (2004) 2614.
[87] E. Sälli, J.-P. Jalkanen, K. Laasonen, L. Halonen,
Mol. Phys. 105 (2007) 1271.
[88] Q.L. Tang, Z.X. Chen, Surf. Sci. 601 (2007) 954.
[89] Q.L. Tang, Z.X. Chen, J. Chem. Phys. 127 (2007) 104707.
[90] S. Walbran, A. Mazzolo, J.W. Halley, D.L. Price,
J. Chem. Phys. 109 (1998) 8076.
[91] S. Wang, Y. Cao, P.A. Rikvold, Phys. Rev. B 70 (2004) 205410.
[92] S. Izvekov, G.A. Voth, J. Chem. Phys. 115 (2001) 7196.
[93] C. Sanchez, Surf. Sci. 527 (2003) 1.
[94] I.C. Yeh, M.L. Berkowitz, Chem. Phys. Lett. 301 (1999) 81.
[95] J. Zhao, C.T. Chan, J.G. Che, Phys. Rev. B 75 (2007) 85435.
[96] M.E. Gallagher, S. Haq, A. Omer, A. Hodgson, Surf. Sci. 601 (2007) 268.
[97] M. Nakamura, M. Ito, Chem. Phys. Lett. 384 (2004) 256.
[98] C. Taylor, R.G. Kelly, M. Neurock, J. Electrochem. Soc. 153 (2006) 207.
[99] A. Michaelides, Appl. Phys. A 85 (2006) 415.
[100] M. Eder, K. Terakura, J. Hafner, Phys. Rev. B 64 (2001) 115426.
[101] R.S. Neves, A.J. Motheo, R.P.S. Fartaria, F.M.S. Silva Fernandes,
J. Electroanal. Chem. 609 (2007) 140.

[102] P. Cabrera Sanfelix, S. Holloway, K.W. Kolasinski, G.R. Darling, Surf. Sci. 532-535 (2003) 166.
[103] J. Li, Y. Li, S. Zhu, F. Wang, Phys. Rev. B 74 (2006) 153415.
[104] M.W. Finnis, R. Kaschner, C. Kruse, J. Furthmuller, M. Scheffler, J. Phys.: Condens. Matter 7 (1995) 2001.
[105] R. Nazmutdinov, T. Zinkicheva, D. Glukhov, M. Shapnik, Russ. J. Electrochem. 39 (2003) 671–678.
[106] R.R. Nazmutdinov, T.T. Zinkicheva, Russ. J. Electrochem. 40 (2004) 379.
[107] A. Hodgson, S. Haq, Surf. Sci. Rep. 64 (2009) 381.
[108] R. Guidelli, W. Schmickler, Electrochim. Acta 45 (2000) 2317.
[109] S. Meng, E.G. Wang, S. Gao, Phys. Rev. B 69 (2004) 195404.
[110] A. Michaelides, V.A. Ranea, P.L. de Andres, D.A. King, Phys. Rev. Lett. 90 (2003) 216102.
[111] A. Shavorskiy, M.J. Gladys, G. Held, Phys. Chem. Chem. Phys. 10 (2008) 6150.
[112] S. Schnur, A. Groß, New J. Phys. 11 (2009) 125003.
[113] A.A. Phatak, W.N. Delgass, F.H. Ribeiro, W.F. Schneider, J. Phys. Chem. C 113 (2009) 7269.
[114] P. Vassilev, R.A. van Santen, M.T.M. Koper, J. Chem. Phys. 122 (2005) 054701.
[115] V. Tripkovic, M.E. Björketun, E. Skúlason, J. Rossmeisl, Phys. Rev. B 84 (2011) 115452.
[116] A. Nilsson, L. Pettersson, J.K. Nørskov, Chemical Bonding at Surfaces and Interfaces, Elsevier, Amsterdam, 2008.
[117] O.A. Petrii, G.A. Tsirlina, in: E. Gileadi, M. Urbakh, A.J. Bard, M. Stratmann (eds) Encyclopedia of Electrochemistry, Vol. 1, Wiley-VCH, Weinheim, 2002.
[118] W. Schmickler, E. Santos, Interfacial Electrochemistry, Oxford University Press, New York, 1996.
[119] E.V. Chulkov, V.M. Silkin, P.M. Echenique, Surf. Sci. 437 (1999) 330.
[120] B. Eck, E. Spohr, Electrochim. Acta 42 (1997) 2779.
[121] D.I. Dimitrov, N.D. Raev, K.I. Semerdzhiev, Phys. Chem. Chem. Phys. 3 (2001) 448.
[122] G. Nagy, K. Heinzinger, J. Electroanal. Chem. 327 (1992) 25.
[123] E. Spohr, Solid State Ionics 150 (2002) 1.
[124] A.N. Frumkin, Potencialy nulevogo zarjada, Nauka, Moskva, 1982.
[125] B.B. Damaskin, A.N. Frumkin, Electrochim. Acta 19 (1974) 173.
[126] W. Ronald Fawcett, P.J. Ryan, J. Electroanal. Chem 649 (2010) 48.
[127] M. Nič, J. Jirát, B. Košata, A. Jenkins, A. McNaught (eds) in: IUPAC Compendium of Chemical Terminology, 2.1.0 ed., IUPAC, Research Triagle Park, NC.
[128] X.-Z. Yuan, C. Song, H. Wang, J. Zhang, Electrochemical Impedance Spectroscopy in PEM Fuel Cells: Fundamentals and Applications, Springer, 2009.

[129] L. Siinor, R. Arendi, K. Lust, E. Lust, In Preparation.
[130] L. Siinor, K. Lust, E. Lust, Electr. Commun. 12 (2010) 1058.
[131] M. Gnahm, C. Müller, R. Répánszki, T. Pajkossy, D.M. Kolb,
Phys. Chem. Chem. Phys. 13 (2011) 11627.
[132] T. Pajkossy, D.M. Kolb, Electr. Commun. 13 (2011) 284.
[133] E. Barsoukov, J.R. Macdonald (eds), Impedance Spectroscopy: Theory,
Experiment, and Applications, Wiley, John & Sons, New Jersey, 2005.
[134] F. Scholz (ed), Electroanalytical Methods: Guide to Experiments and
Applications, Springer, Berlin, 2002.
[135] J.O'M. Bockris, A.K.N. Reddy,
Modern Electrochemistry, Springer-Verlang, Berlin, 2000.
[136] M.S. Kilic, M.Z. Bazant, A. Ajdari, Phys. Rev. E 75 (2007) 021502.
[137] M.S. Kilic, M.Z. Bazant, A. Ajdari, Phys. Rev. E 75 (2007) 021503.
[138] K.B. Oldham, J. Electroanal. Chem. 613 (2008) 131.
[139] D. Jiang, D. Meng, J. Wu, Chem. Phys. Lett. 504 (2011) 153.
[140] J. Forsman, C.E. Woodward, M. Trulsson,
J. Phys. Chem. B 115 (2011) 4606.
[141] J. Wu, T. Jiang, D. Jiang, Z. Jin, D. Henderson,
Soft. Matter. 7 (2011) 11222.
[142] D. Henderson, S. Lamperski, Z. Jin, J. Wu,
J. Phys. Chem. B 115 (2011) 12911.
[143] D. Henderson, S. Lamperski, J. Chem. Eng. Data 56 (2011) 1204.
[144] M.Z. Bazant, B.D. Storey, A.A. Kornyshev,
Phys. Rev. Lett. 106 (2011) 046102.
[145] S.K. Reed, O.J. Lanning, P.A. Madden, J. Chem. Phys. 126 (2007) 084704.
[146] M.V. Fedorov, A.A. Kornyshev, Electrochim. Acta 53 (2008) 6835.
[147] S.A. Kislenko, R.H. Amirov, I.S. Samoylov,
Phys. Chem. Chem. Phys. 12 (2010) 11245.
[148] S. Tazi, M. Salanne, C. Simon, P. Turq, M. Pounds, P.A. Madden,
J. Phys. Chem. B 114 (2010) 8453.
[149] M.V. Fedorov, N. Georgi, A.A. Kornyshev,
Electr. Commun. 12 (2010) 296.
[150] M. Trulsson, J. Algotsson, J. Forsman, C.E. Woodward,
J. Phys. Chem. Lett. 1 (2010) 1191.
[151] J. Vatamanu, O. Borodin, G.D. Smith,
J. Am. Chem. Soc. 132 (2010) 14825.
[152] Q. Dou, M.L. Sha, H.Y. Fu, G.Z. Wu,
J. Phys.: Condens. Matter 23 (2011) 175001.
[153] E. Soolo, D. Brandell, A. Liivat, H. Kasemägi, T. Tamm, A. Aabloo,
J. Mol. Model. 18 (2012) 1541.
[154] B. Roling, M. Drüschler, B. Huber, Faraday Discuss. (2012), In print.
[155] M. Drüschler, N. Borisenko, J. Wallauer, C. Winter, B. Huber, F. Endres,
B. Roling, Phys. Chem. Chem. Phys. 14 (2012) 5090.

[156] M.T. Alam, J. Masud, M.M. Islam, T. Okajima, T. Ohsaka,
J. Phys. Chem. C 115 (2011) 19797.
[157] M. Gnahm, T. Pajkossy, D.M. Kolb, Electrochim. Acta 55 (2010) 6212.
[158] L. Siinor, K. Lust, E. Lust, ECS. Thans. 16 (2009) 559.
[159] F. Silva, C. Gomes, M. Figueiredo, R. Costa, A. Martins, C.M. Pereira,
J. Electroanal. Chem. 622 (2008) 153.
[160] V. Lockett, R. Sedev, J. Ralston, M. Horne, T. Rodopoulos,
J. Phys. Chem. C 112 (2008) 7486.
[161] M.T. Alam, M.M. Islam, T. Okajima, T. Ohsaka,
J. Phys. Chem. C 112 (2008) 16600.
[162] M.M. Islam, M.T. Alam, T. Ohsaka, J. Phys. Chem. C 112 (2008) 16568.
[163] M.M. Islam, M.T. Alam, T. Okajima, T. Ohsaka,
J. Phys. Chem. C 113 (2009) 3386.
[164] R. Costa, C.M. Pereira, F. Silva,
Phys. Chem. Chem. Phys. 12 (2010) 11125.
[165] V. Lockett, M. Horne, R. Sedev, T. Rodopoulos, J. Ralston,
Phys. Chem. Chem. Phys. 12 (2010) 12499.
[166] T.R. Gore, T. Bond, W. Zhang, R.W.J. Scott, I.J. Burgess,
Electr. Commun. 12 (2010) 1340.
[167] M.H. Ghatee, F. Moosavi, J. Phys. Chem. C 115 (2011) 5626.
[168] T.P.C. Klaver, M. Luppi, M.H.F. Sluiter, M.C. Kroon, B.J. Thijsse,
J. Phys. Chem. C 115 (2011) 14718.
[169] H. Valencia, M. Kohyama, S. Tanaka, H. Matsumoto,
J. Chem. Phys. 131 (2009) 244705.
[170] H. Valencia, M. Kohyama, S. Tanaka, H. Matsumoto,
Phys. Rev. B 78 (2008) 205402.
[171] S. Baldelli, Acc. Chem. Res. 41 (2008) 421.
[172] F. Endres, S.Z.E. Abedin, Phys. Chem. Chem. Phys. 8 (2006) 2101.
[173] G.-B. Pan, W. Freyland, Chem. Phys. Lett. 427 (2006) 96.
[174] Y. Su, Y. Fu, J. Yan, Z. Chen, B. Mao, Angew. Chem. 121 (2009) 5250.
[175] N. Borisenko, S. Zein El Abedin, F. Endres, N. Borisenko,
S. Zein El Abedin, F. Endres, Chem. Phys. Chem. 13 (2012) 1736–1742.
[176] F. Endres, N. Borisenko, S.Z.E. Abedin, R. Hayes, R. Atkin,
Faraday Discuss. (2012). In print.
[177] R. Atkin, S.Z.E. Abedin, R. Hayes, L.H.S. Gasparotto, N. Borisenko,
F. Endres, J. Phys. Chem. C 113 (2009) 13266.
[178] R. Atkin, N. Borisenko, M. Drüschler, S.Z. El Abedin, F. Endres,
R. Hayes, B. Huber, B. Roling, Phys. Chem. Chem. Phys. 13 (2011) 6849.
[179] T. Carstens, R. Hayes, S.Z.E. Abedin, B. Corr, G.B. Webber,
N. Borisenko, R. Atkin, F. Endres, Electrochim. Acta (2012). In print.
[180] R. Hayes, N. Borisenko, M.K. Tam, P.C. Howlett, F. Endres, R. Atkin,
J. Phys. Chem. C 115 (2011) 6855.
[181] X. Zhang, Y.-X. Zhong, J.-W. Yan, Y.-Z. Su, M. Zhang, B.-W. Mao,
Chem. Commun. 48 (2012) 582.

[182] R.M. Lynden-Bell, A.I. Frolov, M. Fedorov,
Phys. Chem. Chem. Phys. 14 (2012) 2693.
[183] R. Finken, V. Ballenegger, J.-P. Hansen, Mol. Phys. 101 (2003) 2559.
[184] M. Holovko, V. Kapko, D. Henderson, D. Boda,
Chem. Phys. Lett. 341 (2001) 363.
[185] K. Dong, S. Zhang, Chem. Eur. J. 18 (2012) 2748.
[186] W. Zhao, F. Leroy, B. Heggen, S. Zahn, B. Kirchner, S.Balasubramanian,
F. Müller-Plathe, J. Am. Chem. Soc. 131 (2009) 15825.
[187] G. Feng, J. Huang, B.G. Sumpter, V. Meunier, R. Qiao,
Phys. Chem. Chem. Phys. 13 (2011) 14723.
[188] J. Vatamanu, O. Borodin, G.D. Smith,
J. Am. Chem. Soc. 132 (2010) 14825.
[189] L. Siinor, K. Lust, E. Lust, ECS. Thans. 16 (2009) 559.
[190] J. Zheng, S.S. Moganty, P.C. Goonetilleke, R.E. Baltus, D. Roy,
J. Phys. Chem. C 115 (2011) 7527.

9. Summary in Estonian

Elektrilise kaksikkihi ehitus ja ioonide adsorptsioonikineetika metallelektroodidel toatemperatuuril vedelatest sooladest

Jodiidiooni adsorptsioonikineetika ja 1-etüül-3-metüülimidasoolium tetrafluoroboraadi ($EMImBF_4$) elektrokeemilise käitumise seaduspärasusi Cd(0001) elektroodil uuriti tsüklilise voltamperomeetria ja elektrokeemilise impedantsspektroskoopia meetoditega.

Mõlema uuritava süsteemi korral andis eksperimentaalsete andmete modelleerimisel parimaid tulemusi modifitseeritud Frumkin–Melik-Gaikazyan ekvivalentskeem. Seega võib öelda, et nii vesilahuses kui ka ioonses vedelikus toimub adsorptsiooniprotsess sarnaseid seaduspärasusi järgides, kuigi kõrgsagedusliku mahtuvuse (modelleeritud) väärtused on kahe uuritud süsteemi puhul erinevad. Jodiidioone sisaldava vesilahuse korral temperatuuri tõustes mahtuvuse väärtused vähenevad, mida saab kvalitatiivselt kirjeldada dipoolse võre mudeli abil. Nii tiheduse funktsionaali teooria (DFT) abil saadud arvutustulemused kui ka statistilise-mehaanika meetod viitavad sellele, et temperatuuri kasvades jodiidiooni ja vastava pinnalaengu vaheline vastastikmõju väheneb, mille tulemusel kõrgsageduslik mahtuvus väheneb ning adsorptsiooniline mahtuvus kasvab. Seega elektrilise kaksikkihi tiheda kihi omadused määravad kogu elektrilise kaksikkihi mahtuvusliku käitumise. Vastupidiselt jodiidiooni mahtuvusele $EMImBF_4$ puhul temperatuuri kasvades suureneb ka kõrgsageduslik mahtuvus. Kaasaegsete teoreetiliste mudelite põhjal võib järeldada, et mahtuvuse väärtuse määrab elektrilise kaksikkihi mitmekihiline struktuur metall | ioonne vedelik piirpinnal. Tänu temperatuuri kasvule hakkab ioonide arvatav kihiline struktuur järk-järgult lagunema ning mahtuvus kasvama.

1-etüül-3-metüülimidasoolium tetrafluoroboraadis teistel elektroodidel (Au(111), Bi(111), klaassüsinik) mõõdetud eksperimentaalsete andmete võrdlemisel Cd(0001) elektroodil mõõdetud andmetega selgub, et mahtuvuse väärtused metallelektroodide puhul on ligilähedased, klaassüsinikul mõõdetud mahtuvuse väärtused on aga madalamad. Cd(0001) ja Bi(111) mahtuvuse kõverad $EMImBF_4$-s sõltuvad potentsiaalist erinevalt, seega on need huvitavad süsteemid edaspidisteks DFT arvutusteks.

10. Acknowledgements

First and foremost I would like to express my heartfelt gratitude to scientific consultant prof. Renat R. Nazmutdinov for his continuous warm support throughout my PhD study and for all the advice and great ideas he has been sharing with me.

I am very thankful to Liis Siinor for collaboration in the research, to my FRIENDS Aleksei Lissitsin, Katerina Štšogoleva, and Oleg Košik for their support, as well as to all my colleagues in the University of Tartu for the helpful and warm atmosphere. I am extremely grateful to Jekaterina Jeromenok, Jörgen Metsik, Jüri Hudoleev, Steven Frayne, and my students Ove Oll and Anton Ruzanov for proofreading of the manuscript. I wish to thank my beloved mother, father and sister for their support and encouragement throughout my study.

Last but not least, I am very thankful to prof. Enn Lust and PhD Karmen Lust, my research supervisors, for their patient guidance, enthusiastic encouragement and useful critiques of this research work.

The presented experimental studies were performed at the Institute of Chemistry, while the calculations at a cluster in the Institute of Physics of the University of Tartu. I would also like to extend my thanks to the technicians of the Institute of Physics for their help in offering me the computational resources. The support received from Estonian Science Foundation (grant ETF8357), from Centre of Excellence (project TK117) and from Graduate School „Functional materials and technologies“ receiving funding from the European Social Fund under project 1.2.0401.09-0079 are acknowledged.

11. Publications

Curriculum Vitae

Vladislav Ivaništšev

Born:	04. april 1984, Severobaikalsk, Russian Federation
Address:	University of Tartu, Institute on chemistry, Ravila, 14A, Tartu 50411, Eesti
E-mail:	vladislav.ivanistsev@ut.ee

Education

2008–...	University of Tartu, Ph.D. student
2006–2008	University of Tartu, M.Sc. in physical- and electrochemistry
2003–2006	University of Tartu, B.Sc. in physical- and electrochemistry

Professional employment and retraining

2005–2006	University of Tartu, Institute of Chemistry, laboratory assistant
2006–2012	University of Tartu, Institute of Chemistry, engineer

Professional employment

2010	Technical University of Denmark (Prof. J. Rossmeisl) Lyngby, Copenhagen (Denmark), 6 months
2011	Technical University of Kazan (Prof. R.R. Nazmutdinov) Kazan (Russian Federation), 2 weeks
2010	Technical University of Denmark (Prof. J. Rossmeisl) Lyngby, Copenhagen (Denmark), 2 weeks

List of publications

1) V. Ivaništšev, R.R. Nazmutdinov, E. Lust, A comparative DFT study of the adsorption of H_2O molecules at Bi, Hg, and Ga surfaces.
Submitted to the Journal "Surface Science".

2) L. Siinor, C. Siimenson, V. Ivaništšev, K. Lust, E. Lust, Influence of cation chemical composition and structure on the double layer capacitance for Bi(111) | room temperature ionic liquid interface.
Journal of Electroanalytical Chemistry 668 (2012) 30-36.

3) V. Ivaništšev, R.R. Nazmutdinov, E. Lust, Density functional theory study of the water adsorption at Bi(111) electrode surface.
Surface Science 604 (2010) 1919-1927.

4) L. Siinor, V. Ivaništšev, K. Lust, E. Lust, Impedance study of adsorption of iodide ions at Cd(0001) and Bi(111) electrode from various solutions with constant ionic strength.
Journal of Solid State Electrochemistry, 14 (2010) 555-563.

Conference abstracts and presentations

1) V. Ivaništšev, K. Lust (2006), Adsorption kinetics of iodide ions on the electrochemically polished Cd and Bi single crystal electrodes. Innovative Electrochemistry, Enterprising Science: 57th Annual Meeting of the International society of Electrochemistry; Edinburgh, UK; 27 August–1 September 2006, S8-P-48.

2) V. Ivaništšev, K. Lust (2008), Adsorption kinetics of iodide ions on the cadmium (0001) single crystal electrode from different base electrolyte solutions. 5th Baltic Conference on Electrochemistry; Tartu, Estonia; 30 april–3 May 2008, P-15.

3) V. Ivaništšev, R.R. Nazmutdinov, E. Lust (2009). A DFT study of the water adsorption at a Bi(111) electrode surface. Emerging Trends and Challenges in Electrochemistry: 60th Annual Meeting of the International Society of Electrochemistry; Beijing, P. R. China; 16–21 August 2009, presentation.

4) V. Ivaništšev, R.R. Nazmutdinov, E. Lust (2009). DFT study of water adsorption on Bi(111): Effect of applied electric field. 12-th Session of the V.A. Fock Meeting on Quantum and Computational Chemistry; Kazan, Russian Federation, 19–23 October 2009, Nr. 1696.

5) V. Ivaništšev, R.R. Nazmutdinov, E. Lust, A DFT study of the water adsorption at Bi, Hg, and Ga electrode surfaces. Electrochemistry from Biology to Physics: 61th Annual Meeting of the International society of Electrochemistry; Nice, France; 26 September–1 October 2010, 2010, s15-P-004.

6) V. Ivaništšev, J. Rossmeisl, Ab initio study of the electrified Au(111) | EMIM–BF_4 ionic liquid interface. Ψ_k-2010 Conference; Berlin, Germany; 12–16 September, 2010, S13-P229

7) K. Lust, L. Siinor, C. Siimenson, V. Ivaništšev, A. Ruzanov, E. Lust (2012), Double Layer Structure at the Bi(*hkl*)- and Cd(*hklf*) -electrolyte Interfaces. Electrochemical Frontiers in Global Environment and Energy: 62th Annual Meeting of the International Society of Electrochemistry; Niigata, Japan,11–16 September 2011, presentation.

8) V. Ivaništšev, Ove Oll, R.R. Nazmutdinov (2012). A quantum chemical study of the interaction of ionic liquids with a Bi(111) surface. 13-th Session of the V.A. Fock Meeting on Quantum and Computational Chemistry; Astana, Kazakhstan, 23–27 April 2012, Nr. 1786.

9) V. Ivaništšev, R.R. Nazmutdinov (2012). A DFT study of the adsorption of aromatic molecules at a Bi(111) surface by using long range-corrected functionals. 13-th Session of the V.A. Fock Meeting on Quantum and Computational Chemistry; Astana, Kazakhstan, 23–27 April 2012, Nr. 1835.

10) S.N. Srirama, C. Willmore, V. Ivanistsev, P. Jakovits and U. Norbisrath (2012). Desktop to Cloud Migration of Scientific Experiments. 2nd International Workshop on Cloud Computing and Scientific Applications (CCSA) held in conjunction with the 12th IEEE/ACM International Symposium on Cluster, Cloud and Grid Computing (CCGrid 2012); Ottawa, Canada, 13–16 May 2012, presentation. The paper is invited for the Special Issue of Future Generation Computer Systems (FGCS).

11) V. Ivaništšev, J. Rossmeisl (2012). DFT study of potential-dependent iodide adsorption at Au(111) electrode. Theoretical and Computational Electrochemistry: 11th Spring Meeting of the International Society of Electrochemistry. Georgetown, Washington, DC, USA, 23–25 May, 2012, P-015.

12) V. Ivaništšev, R.R. Nazmutdinov, E. Lust (2012), Influence of cation chemical composition and structure on the specific interactions at Bi(111) | room temperature ionic liquid interface. Theoretical and Computational Electrochemistry: 11th Spring Meeting of the International Society of Electrochemistry. Georgetown, Washington, DC, USA, 23–25 May, 2012, P-024.

Elulookirjeldus

Vladislav Ivaništšev

Sünniaeg ja koht: 04. aprill 1984, Severobaikalsk, Venemaa
Aadress: Tartu Ülikool, Keemia Instituut, Ravila, 14A, Tartu 50411, Eesti
E-mail: vladislav.ivanistsev@ut.ee

Haridus

2008–...	Tartu Ülikooli, Keemia Instituut, Doktoriõpe
2006–2008	Tartu Ülikooli, Füüsika-keemiateaduskond, keemia eriala, Magistriõpe
2003–2006	Tartu Ülikooli, Füüsika-keemiateaduskond, keemia eriala, Bakalaureuseõpe

Teemistuskäik

2005–2006	Tartu Ülikool, Füüsika-keemiateaduskond, laborant
2006–2012	Tartu Ülikool, Keemia Instituut, insener

Erialane enesetäiendus

2010	Technical University of Denmark (Prof. J. Rossmeisl) Lyngby, Copenhagen (Denmark), 6 kuud
2011	Technical University of Kazan (Prof. R.R. Nazmutdinov Kazan (Russian Federation), 2 nädalat
2010	Technical University of Denmark (Prof. J. Rossmeisl) Lyngby, Copenhagen (Denmark), 2 nädalat

Teaduspublikatsioonid

1) V. Ivaništšev, R.R. Nazmutdinov, E. Lust, A comparative DFT study of the adsorption of H_2O molecules at Bi, Hg, and Ga surfaces.
Submitted to the Journal "Surface Science".
2) L. Siinor, C. Siimenson, V. Ivaništšev, K. Lust, E. Lust, Influence of cation chemical composition and structure on the double layer capacitance for Bi(111) | room temperature ionic liquid interface.
Journal of Electroanalytical Chemistry 668 (2012) 30-36.
3) V. Ivaništšev, R.R. Nazmutdinov, E. Lust, Density functional theory study of the water adsorption at Bi(111) electrode surface.
Surface Science 604 (2010) 1919-1927.
4) L. Siinor, V. Ivaništšev, K. Lust, E. Lust, Impedance study of adsorption of iodide ions at Cd(0001) and Bi(111) electrode from various solutions with constant ionic strength.
Journal of Solid State Electrochemistry, 14 (2010) 555-563.

Konverentsi teesid ja ettekanned

1) V. Ivaništšev, K. Lust (2006), Adsorption kinetics of iodide ions on the electrochemically polished Cd and Bi single crystal electrodes. Innovative Electrochemistry, Enterprising Science: 57th Annual Meeting of the International society of Electrochemistry; Edinburgh, UK; 27 August–1 September 2006, S8-P-48.

2) V. Ivaništšev, K. Lust (2008), Adsorption kinetics of iodide ions on the cadmium (0001) single crystal electrode from different base electrolyte solutions. 5th Baltic Conference on Electrochemistry; Tartu, Estonia; 30 april–3 May 2008, P-15.

3) V. Ivaništšev, R.R. Nazmutdinov, E. Lust (2009). A DFT study of the water adsorption at a Bi(111) electrode surface. Emerging Trends and Challenges in Electrochemistry: 60th Annual Meeting of the International Society of Electrochemistry; Beijing, P. R. China; 16–21 August 2009, presentation.

4) V. Ivaništšev, R.R. Nazmutdinov, E. Lust (2009). DFT study of water adsorption on Bi(111): Effect of applied electric field. 12-th Session of the V.A. Fock Meeting on Quantum and Computational Chemistry; Kazan, Russian Federation, 19–23 October 2009, Nr. 1696.

5) V. Ivaništšev, R.R. Nazmutdinov, E. Lust, A DFT study of the water adsorption at Bi, Hg, and Ga electrode surfaces. Electrochemistry from Biology to Physics: 61th Annual Meeting of the International society of Electrochemistry; Nice, France; 26 September–1 October 2010, 2010, s15-P-004.

6) V. Ivaništšev, J. Rossmeisl, Ab initio study of the electrified Au(111) | EMIM–BF_4 ionic liquid interface. Ψ_k-2010 Conference; Berlin, Germany; 12–16 September, 2010, S13-P229

7) K. Lust, L. Siinor, C. Siimenson, V. Ivaništšev, A. Ruzanov, E. Lust (2012), Double Layer Structure at the Bi(*hkl*)- and Cd(*hklf*) -electrolyte Interfaces. Electrochemical Frontiers in Global Environment and Energy: 62th Annual Meeting of the International Society of Electrochemistry; Niigata, Japan,11–16 September 2011, presentation.

8) V. Ivaništšev, Ove Oll, R.R. Nazmutdinov (2012). A quantum chemical study of the interaction of ionic liquids with a Bi(111) surface. 13-th Session of the V.A. Fock Meeting on Quantum and Computational Chemistry; Astana, Kazakhstan, 23–27 April 2012, Nr. 1786.

9) V. Ivaništšev, R.R. Nazmutdinov (2012). A DFT study of the adsorption of aromatic molecules at a Bi(111) surface by using long range-corrected functionals. 13-th Session of the V.A. Fock Meeting on Quantum and Computational Chemistry; Astana, Kazakhstan, 23–27 April 2012, Nr. 1835.

10) S.N. Srirama, C. Willmore, V. Ivanistsev, P. Jakovits and U. Norbisrath (2012). Desktop to Cloud Migration of Scientific Experiments. 2nd International Workshop on Cloud Computing and Scientific Applications (CCSA) held in conjunction with the 12th IEEE/ACM International Symposium on Cluster, Cloud and Grid Computing (CCGrid 2012); Ottawa, Canada, 13–16 May 2012, presentation. The paper is invited for the Special Issue of Future Generation Computer Systems (FGCS).

11) V. Ivaništšev, J. Rossmeisl (2012). DFT study of potential-dependent iodide adsorption at Au(111) electrode. Theoretical and Computational Electrochemistry: 11th Spring Meeting of the International Society of Electrochemistry. Georgetown, Washington, DC, USA, 23–25 May, 2012, P-015.

12) V. Ivaništšev, R.R. Nazmutdinov, E. Lust (2012), Influence of cation chemical composition and structure on the specific interactions at Bi(111) | room temperature ionic liquid interface. Theoretical and Computational Electrochemistry: 11th Spring Meeting of the International Society of Electrochemistry. Georgetown, Washington, DC, USA, 23–25 May, 2012, P-024.

DISSERTATIONES CHIMICAE UNIVERSITATIS TARTUENSIS

1. **Toomas Tamm.** Quantum-chemical simulation of solvent effects. Tartu, 1993, 110 p.
2. **Peeter Burk.** Theoretical study of gas-phase acid-base equilibria. Tartu, 1994, 96 p.
3. **Victor Lobanov.** Quantitative structure-property relationships in large descriptor spaces. Tartu, 1995, 135 p.
4. **Vahur Mäemets.** The ^{17}O and ^{1}H nuclear magnetic resonance study of H_2O in individual solvents and its charged clusters in aqueous solutions of electrolytes. Tartu, 1997, 140 p.
5. **Andrus Metsala.** Microcanonical rate constant in nonequilibrium distribution of vibrational energy and in restricted intramolecular vibrational energy redistribution on the basis of slater's theory of unimolecular reactions. Tartu, 1997, 150 p.
6. **Uko Maran.** Quantum-mechanical study of potential energy surfaces in different environments. Tartu, 1997, 137 p.
7. **Alar Jänes.** Adsorption of organic compounds on antimony, bismuth and cadmium electrodes. Tartu, 1998, 219 p.
8. **Kaido Tammeveski.** Oxygen electroreduction on thin platinum films and the electrochemical detection of superoxide anion. Tartu, 1998, 139 p.
9. **Ivo Leito.** Studies of Brønsted acid-base equilibria in water and non-aqueous media. Tartu, 1998, 101 p.
10. **Jaan Leis.** Conformational dynamics and equilibria in amides. Tartu, 1998, 131 p.
11. **Toonika Rinken.** The modelling of amperometric biosensors based on oxidoreductases. Tartu, 2000, 108 p.
12. **Dmitri Panov.** Partially solvated Grignard reagents. Tartu, 2000, 64 p.
13. **Kaja Orupõld.** Treatment and analysis of phenolic wastewater with microorganisms. Tartu, 2000, 123 p.
14. **Jüri Ivask.** Ion Chromatographic determination of major anions and cations in polar ice core. Tartu, 2000, 85 p.
15. **Lauri Vares.** Stereoselective Synthesis of Tetrahydrofuran and Tetrahydropyran Derivatives by Use of Asymmetric Horner-Wadsworth-Emmons and Ring Closure Reactions. Tartu, 2000, 184 p.
16. **Martin Lepiku.** Kinetic aspects of dopamine D_2 receptor interactions with specific ligands. Tartu, 2000, 81 p.
17. **Katrin Sak.** Some aspects of ligand specificity of P2Y receptors. Tartu, 2000, 106 p.
18. **Vello Pällin.** The role of solvation in the formation of iotsitch complexes. Tartu, 2001, 95 p.

19. **Katrin Kollist.** Interactions between polycyclic aromatic compounds and humic substances. Tartu, 2001, 93 p.
20. **Ivar Koppel.** Quantum chemical study of acidity of strong and superstrong Brønsted acids. Tartu, 2001, 104 p.
21. **Viljar Pihl.** The study of the substituent and solvent effects on the acidity of OH and CH acids. Tartu, 2001, 132 p.
22. **Natalia Palm.** Specification of the minimum, sufficient and significant set of descriptors for general description of solvent effects. Tartu, 2001, 134 p.
23. **Sulev Sild.** QSPR/QSAR approaches for complex molecular systems. Tartu, 2001, 134 p.
24. **Ruslan Petrukhin.** Industrial applications of the quantitative structure-property relationships. Tartu, 2001, 162 p.
25. **Boris V. Rogovoy.** Synthesis of (benzotriazolyl)carboximidamides and their application in relations with *N*- and *S*-nucleophyles. Tartu, 2002, 84 p.
26. **Koit Herodes.** Solvent effects on UV-vis absorption spectra of some solvatochromic substances in binary solvent mixtures: the preferential solvation model. Tartu, 2002, 102 p.
27. **Anti Perkson.** Synthesis and characterisation of nanostructured carbon. Tartu, 2002, 152 p.
28. **Ivari Kaljurand.** Self-consistent acidity scales of neutral and cationic Brønsted acids in acetonitrile and tetrahydrofuran. Tartu, 2003, 108 p.
29. **Karmen Lust.** Adsorption of anions on bismuth single crystal electrodes. Tartu, 2003, 128 p.
30. **Mare Piirsalu.** Substituent, temperature and solvent effects on the alkaline hydrolysis of substituted phenyl and alkyl esters of benzoic acid. Tartu, 2003, 156 p.
31. **Meeri Sassian.** Reactions of partially solvated Grignard reagents. Tartu, 2003, 78 p.
32. **Tarmo Tamm.** Quantum chemical modelling of polypyrrole. Tartu, 2003. 100 p.
33. **Erik Teinemaa.** The environmental fate of the particulate matter and organic pollutants from an oil shale power plant. Tartu, 2003. 102 p.
34. **Jaana Tammiku-Taul.** Quantum chemical study of the properties of Grignard reagents. Tartu, 2003. 120 p.
35. **Andre Lomaka.** Biomedical applications of predictive computational chemistry. Tartu, 2003. 132 p.
36. **Kostyantyn Kirichenko.** Benzotriazole – Mediated Carbon–Carbon Bond Formation. Tartu, 2003. 132 p.
37. **Gunnar Nurk.** Adsorption kinetics of some organic compounds on bismuth single crystal electrodes. Tartu, 2003, 170 p.
38. **Mati Arulepp.** Electrochemical characteristics of porous carbon materials and electrical double layer capacitors. Tartu, 2003, 196 p.

39. **Dan Cornel Fara.** QSPR modeling of complexation and distribution of organic compounds. Tartu, 2004, 126 p.
40. **Riina Mahlapuu.** Signalling of galanin and amyloid precursor protein through adenylate cyclase. Tartu, 2004, 124 p.
41. **Mihkel Kerikmäe.** Some luminescent materials for dosimetric applications and physical research. Tartu, 2004, 143 p.
42. **Jaanus Kruusma.** Determination of some important trace metal ions in human blood. Tartu, 2004, 115 p.
43. **Urmas Johanson.** Investigations of the electrochemical properties of polypyrrole modified electrodes. Tartu, 2004, 91 p.
44. **Kaido Sillar.** Computational study of the acid sites in zeolite ZSM-5. Tartu, 2004, 80 p.
45. **Aldo Oras.** Kinetic aspects of dATPαS interaction with $P2Y_1$ receptor. Tartu, 2004, 75 p.
46. **Erik Mölder.** Measurement of the oxygen mass transfer through the air-water interface. Tartu, 2005, 73 p.
47. **Thomas Thomberg.** The kinetics of electroreduction of peroxodisulfate anion on cadmium (0001) single crystal electrode. Tartu, 2005, 95 p.
48. **Olavi Loog.** Aspects of condensations of carbonyl compounds and their imine analogues. Tartu, 2005, 83 p.
49. **Siim Salmar.** Effect of ultrasound on ester hydrolysis in aqueous ethanol. Tartu, 2006, 73 p.
50. **Ain Uustare.** Modulation of signal transduction of heptahelical receptors by other receptors and G proteins. Tartu, 2006, 121 p.
51. **Sergei Yurchenko.** Determination of some carcinogenic contaminants in food. Tartu, 2006, 143 p.
52. **Kaido Tämm.** QSPR modeling of some properties of organic compounds. Tartu, 2006, 67 p.
53. **Olga Tšubrik.** New methods in the synthesis of multisubstituted hydrazines. Tartu. 2006, 183 p.
54. **Lilli Sooväli.** Spectrophotometric measurements and their uncertainty in chemical analysis and dissociation constant measurements. Tartu, 2006, 125 p.
55. **Eve Koort.** Uncertainty estimation of potentiometrically measured ph and pK_a values. Tartu, 2006, 139 p.
56. **Sergei Kopanchuk.** Regulation of ligand binding to melanocortin receptor subtypes. Tartu, 2006, 119 p.
57. **Silvar Kallip.** Surface structure of some bismuth and antimony single crystal electrodes. Tartu, 2006, 107 p.
58. **Kristjan Saal.** Surface silanization and its application in biomolecule coupling. Tartu, 2006, 77 p.
59. **Tanel Tätte.** High viscosity $Sn(OBu)_4$ oligomeric concentrates and their applications in technology. Tartu, 2006, 91 p.

60. **Dimitar Atanasov Dobchev**. Robust QSAR methods for the prediction of properties from molecular structure. Tartu, 2006, 118 p.
61. **Hannes Hagu**. Impact of ultrasound on hydrophobic interactions in solutions. Tartu, 2007, 81 p.
62. **Rutha Jäger.** Electroreduction of peroxodisulfate anion on bismuth electrodes. Tartu, 2007, 142 p.
63. **Kaido Viht.** Immobilizable bisubstrate-analogue inhibitors of basophilic protein kinases: development and application in biosensors. Tartu, 2007, 88 p.
64. **Eva-Ingrid Rõõm.** Acid-base equilibria in nonpolar media. Tartu, 2007, 156 p.
65. **Sven Tamp.** DFT study of the cesium cation containing complexes relevant to the cesium cation binding by the humic acids. Tartu, 2007, 102 p.
66. **Jaak Nerut.** Electroreduction of hexacyanoferrate(III) anion on Cadmium (0001) single crystal electrode. Tartu, 2007, 180 p.
67. **Lauri Jalukse.** Measurement uncertainty estimation in amperometric dissolved oxygen concentration measurement. Tartu, 2007, 112 p.
68. **Aime Lust.** Charge state of dopants and ordered clusters formation in CaF_2:Mn and CaF_2:Eu luminophors. Tartu, 2007, 100 p.
69. **Iiris Kahn**. Quantitative Structure-Activity Relationships of environmentally relevant properties. Tartu, 2007, 98 p.
70. **Mari Reinik.** Nitrates, nitrites, N-nitrosamines and polycyclic aromatic hydrocarbons in food: analytical methods, occurrence and dietary intake. Tartu, 2007, 172 p.
71. **Heili Kasuk.** Thermodynamic parameters and adsorption kinetics of organic compounds forming the compact adsorption layer at Bi single crystal electrodes. Tartu, 2007, 212 p.
72. **Erki Enkvist.** Synthesis of adenosine-peptide conjugates for biological applications. Tartu, 2007, 114 p.
73. **Svetoslav Hristov Slavov**. Biomedical applications of the QSAR approach. Tartu, 2007, 146 p.
74. **Eneli Härk.** Electroreduction of complex cations on electrochemically polished Bi(*hkl*) single crystal electrodes. Tartu, 2008, 158 p.
75. **Priit Möller.** Electrochemical characteristics of some cathodes for medium temperature solid oxide fuel cells, synthesized by solid state reaction technique. Tartu, 2008, 90 p.
76. **Signe Viggor.** Impact of biochemical parameters of genetically different pseudomonads at the degradation of phenolic compounds. Tartu, 2008, 122 p.
77. **Ave Sarapuu.** Electrochemical reduction of oxygen on quinone-modified carbon electrodes and on thin films of platinum and gold. Tartu, 2008, 134 p.
78. **Agnes Kütt.** Studies of acid-base equilibria in non-aqueous media. Tartu, 2008, 198 p.

79. **Rouvim Kadis.** Evaluation of measurement uncertainty in analytical chemistry: related concepts and some points of misinterpretation. Tartu, 2008, 118 p.
80. **Valter Reedo.** Elaboration of IVB group metal oxide structures and their possible applications. Tartu, 2008, 98 p.
81. **Aleksei Kuznetsov.** Allosteric effects in reactions catalyzed by the cAMP-dependent protein kinase catalytic subunit. Tartu, 2009, 133 p.
82. **Aleksei Bredihhin.** Use of mono- and polyanions in the synthesis of multisubstituted hydrazine derivatives. Tartu, 2009, 105 p.
83. **Anu Ploom.** Quantitative structure-reactivity analysis in organosilicon chemistry. Tartu, 2009, 99 p.
84. **Argo Vonk.** Determination of adenosine A_{2A}- and dopamine D_1 receptor-specific modulation of adenylate cyclase activity in rat striatum. Tartu, 2009, 129 p.
85. **Indrek Kivi.** Synthesis and electrochemical characterization of porous cathode materials for intermediate temperature solid oxide fuel cells. Tartu, 2009, 177 p.
86. **Jaanus Eskusson.** Synthesis and characterisation of diamond-like carbon thin films prepared by pulsed laser deposition method. Tartu, 2009, 117 p.
87. **Marko Lätt.** Carbide derived microporous carbon and electrical double layer capacitors. Tartu, 2009, 107 p.
88. **Vladimir Stepanov.** Slow conformational changes in dopamine transporter interaction with its ligands. Tartu, 2009, 103 p.
89. **Aleksander Trummal.** Computational Study of Structural and Solvent Effects on Acidities of Some Brønsted Acids. Tartu, 2009, 103 p.
90. **Eerold Vellemäe.** Applications of mischmetal in organic synthesis. Tartu, 2009, 93 p.
91. **Sven Parkel.** Ligand binding to 5-HT_{1A} receptors and its regulation by Mg^{2+} and Mn^{2+}. Tartu, 2010, 99 p.
92. **Signe Vahur.** Expanding the possibilities of ATR-FT-IR spectroscopy in determination of inorganic pigments. Tartu, 2010, 184 p.
93. **Tavo Romann**. Preparation and surface modification of bismuth thin film, porous, and microelectrodes. Tartu, 2010, 155 p.
94. **Nadežda Aleksejeva.** Electrocatalytic reduction of oxygen on carbon nanotube-based nanocomposite materials. Tartu, 2010, 147 p.
95. **Marko Kullapere.** Electrochemical properties of glassy carbon, nickel and gold electrodes modified with aryl groups. Tartu, 2010, 233 p.
96. **Liis Siinor.** Adsorption kinetics of ions at Bi single crystal planes from aqueous electrolyte solutions and room-temperature ionic liquids. Tartu, 2010, 101 p.
97. **Angela Vaasa.** Development of fluorescence-based kinetic and binding assays for characterization of protein kinases and their inhibitors. Tartu 2010, 101 p.

98. **Indrek Tulp.** Multivariate analysis of chemical and biological properties. Tartu 2010, 105 p.
99. **Aare Selberg.** Evaluation of environmental quality in Northern Estonia by the analysis of leachate. Tartu 2010, 117 p.
100. **Darja Lavõgina.** Development of protein kinase inhibitors based on adenosine analogue-oligoarginine conjugates. Tartu 2010, 248 p.
101. **Laura Herm.** Biochemistry of dopamine D_2 receptors and its association with motivated behaviour. Tartu 2010, 156 p.
102. **Terje Raudsepp.** Influence of dopant anions on the electrochemical properties of polypyrrole films. Tartu 2010, 112 p.
103. **Margus Marandi.** Electroformation of Polypyrrole Films: *In-situ* AFM and STM Study. Tartu 2011, 116 p.
104. **Kairi Kivirand.** Diamine oxidase-based biosensors: construction and working principles. Tartu, 2011, 140 p.
105. **Anneli Kruve.** Matrix effects in liquid-chromatography electrospray mass-spectrometry. Tartu, 2011, 156 p.
106. **Gary Urb.** Assessment of environmental impact of oil shale fly ash from PF and CFB combustion. Tartu, 2011, 108 p.
107. **Nikita Oskolkov.** A novel strategy for peptide-mediated cellular delivery and induction of endosomal escape. Tartu, 2011, 106 p.
108. **Dana Martin.** The QSPR/QSAR approach for the prediction of properties of fullerene derivatives. Tartu, 2011, 98 p.
109. **Säde Viirlaid.** Novel glutathione analogues and their antioxidant activity. Tartu, 2011, 106 p.
110. **Ülis Sõukand.** Simultaneous adsorption of Cd^{2+}, Ni^{2+}, and Pb^{2+} on peat. Tartu, 2011, 124 p.
111. **Lauri Lipping.** The acidity of strong and superstrong Brønsted acids, an outreach for the "limits of growth": a quantum chemical study. Tartu, 2011, 124 p.
112. **Heisi Kurig.** Electrical double-layer capacitors based on ionic liquids as electrolytes. Tartu, 2011, 146 p.
113. **Marje Kasari.** Bisubstrate luminescent probes, optical sensors and affinity adsorbents for measurement of active protein kinases in biological samples. Tartu, 2012, 126 p.
114. **Kalev Takkis.** Virtual screening of chemical databases for bioactive molecules. Tartu, 2012, 122 p.
115. **Ksenija Kisseljova**. Synthesis of aza-β^3-amino acid containing peptides and kinetic study of their phosphorylation by protein kinase A. Tartu, 2012, 104 p.
116. **Riin Rebane.** Advanced method development strategy for derivatization LC/ESI/MS. Tartu, 2012, 184 p.